INSIGHTS INTO ASTROPHYLLITE-GROUP MINERALS. II. CRYSTAL CHEMISTRY

Paula C. PIILONEN§

*Ottawa–Carleton Geoscience Centre, Department of Earth Sciences, University of Ottawa,
Ottawa, Ontario K1N 6N5, Canada*

Andrew M. McDONALD

Department of Earth Sciences, Laurentian University, Sudbury, Ontario P3E 2C6, Canada

André E. LALONDE

*Ottawa–Carleton Geoscience Centre, Department of Earth Sciences, University of Ottawa,
Ottawa, Ontario K1N 6N5, Canada*

Abstract

The crystal chemistry of 20 specimens of astrophyllite-group minerals from seven localities has been studied using a combination of single-crystal X-ray analysis of the structure and electron-microprobe analyses. Members of the astrophyllite group are triclinic ($P\bar{1}$) and monoclinic ($C2/c$ or $A2$) heterophyllosilicates with the general formula $A_2BC_7D_2T_8O_{26}(OH)_4X_{0-1}$, where A = $^{[10]-[13]}$K, Rb, Cs, Na, H_3O^+, H_2O, or $\square$; B = $^{[10]}$Na or Ca; C = $^{[6]}$Mn, Fe^{2+}, Fe^{3+}, Na, Mg, or Zn; D = $^{[6]}$Ti, Nb, or Zr; T = Si and Al, and X = F, OH, O, or $\square$. The structure consists of two composite sheets, a heterogeneous (H) sheet and a sheet of octahedra (O), stacked along [001] in a 2:1 ratio. These 2:1 composite layers are bonded *via* a shared apical $D\phi_6$ anion through an interlayer containing an ordered array of K and Na, resulting in a layered *HOH* structure reminiscent of the *TOT* structure in 2:1 phyllosilicates. There are four crystallographically distinct MO_6 octahedra in the O sheet; they host Mn, Fe^{2+}, Fe^{3+}, Na, Mg and Zn. The $M(1)$ octahedron, the largest and least distorted within the O sheet, is host predominantly to Mn and Fe^{2+}, with significant Na (up to 0.274 *apfu*). The $M(2)$ octahedron is highly distorted and contains predominantly Mn and Fe^{2+}, whereas the $M(3)$ and $M(4)$ octahedra are the smallest and are occupied by Mn, Fe^{2+}, Fe^{3+}, Mg and Zn. The H sheet consists of open-branched *zweier* [100] single $[Si_4O_{12}]^{8-}$ chains cross-linked by corner-sharing $D\phi_6$ octahedra in triclinic species and kupletskite-$Ma2b2c$, and DO_5 polyhedra in magnesium astrophyllite. Distortion of the $D\phi_6$ octahedron is minimized by (Nb,Zr) ⇔ Ti substitution, resulting in displacement of the cation toward the center of the octahedron. The composition of the $[Si_4O_{12}]^{8-}$ chains does not vary; there is essentially no Al, and Mössbauer spectroscopy did not indicate the presence of $^{[4]}Fe^{3+}$. Lateral fit of the O and H sheets is accomplished primarily by: (1) flattening of O-sheet octahedra, (2) tilting of the H-sheet tetrahedra out of the (001) plane, and (3) elongation or thickening of the tetrahedra along [001].

Keywords: astrophyllite-group minerals, crystal structure, crystal chemistry, heterophyllosilicates.

Sommaire

Nous avons étudié la cristallochimie de vingt échantillons de minéraux du groupe de l'astrophyllite provenant de sept endroits en utilisant une combinaison d'analyse structurale par diffraction X portant sur monocristal et analyse chimique avec une microsonde électronique. Les minéraux de ce groupe sont des hétérophyllosilicates tricliniques ($P\bar{1}$) ou monocliniques ($C2/c$ ou $A2$) répondant à la formule générale $A_2BC_7D_2T_8O_{26}(OH)_4X_{0-1}$, dans laquelle A = $^{[10]-[13]}$K, Rb, Cs, Na, H_3O^+, H_2O, ou $\square$; B = $^{[10]}$Na ou Ca; C = $^{[6]}$Mn, Fe^{2+}, Fe^{3+}, Na, Mg, ou Zn; D = $^{[6]}$Ti, Nb, ou Zr; T = Si et Al, et X = F, OH, O, ou $\square$. La structure conprend deux feuillets composites, un feuillet hétérogène (H) et un feuillet d'octaèdres (O), empilés le long de [001] dans un rapport 2:1. Ces feuillets composites 2:1 sont interliés grâce au partage d'un anion apical $D\phi_6$ dans un interfeuillet contenant une distribution ordonnée de K et de Na, avec comme résultat une structure *HOH* en couches ressemblant à la structure *TOT* dans les phyllosilicates. Il y a quatre octaèdres MO_6 cristallographiquement distincts dans le feuillet O; ils renferment Mn, Fe^{2+}, Fe^{3+}, Na, Mg et Zn. L'octaèdre $M(1)$, le plus volumineux et le moins difforme, renferme surtout Mn et Fe^{2+}, avec une fraction importante de Na (jusqu'à 0.274 atomes par unité formulaire. L'octaèdre $M(2)$ est fortement difforme et contient surtout Mn et Fe^{2+}, tandis que

---
§ *Current address*: Research Division, Canadian Museum of Nature, P.O. Box 3443, Station D, Ottawa, Ontario K1P 6P4, Canada. *E-mail address*: ppiilonen@mus-nature.ca

$M(3)$ et $M(4)$ sont les plus petits et renferment Mn, Fe^{2+}, Fe^{3+}, Mg et Zn. Le feuillet H est fait d'un embranchement ouvert *zweier* [100] de chaînes simples $[Si_4O_{12}]^{8-}$ interliées par partage de coins d'un octaèdre $D\phi_6$ dans les espèces tricliniques et la kupletskite-$Ma2b2c$, ou d'un polyèdre DO_5 dans la magnésium astrophyllite. La distortion de l'octaèdre $D\phi_6$ est minimisée par une substitution (Nb,Zr) ⇔ Ti, et un déplacement du cation vers le centre de l'octaèdre. La composition des chaînes $[Si_4O_{12}]^{8-}$ ne varie pas; il n'y a presque pas d'aluminium, et les spectres de Mössbauer excluent la présence de $^{[4]}Fe^{3+}$. La concordance des dimensions latérales des feuillets O et H se fait principalement par: (1) applatissement des octaèdres du feuillet O, (2) inclinaison des tétraèdres du feuillet H par rapport au plan (001), et (3) allongement ou épaississement des tétraèdres le long de [001].

(Traduit par la Rédaction)

Mots-clés: minéraux du groupe de l'astrophyllite, structure cristalline, cristallochimie, hétérophyllosilicates.

INTRODUCTION

Astrophyllite-group minerals are alkali titano-, niobo- and zirconosilicates that crystallize in peralkaline nepheline syenites, their associated pegmatites, alkali granites, and their metamorphic equivalents. Piilonen *et al.* (2003) described the extensive variability in chemical composition observed in such minerals from silica oversaturated and undersaturated intrusions, a reflection of a crystal structure that contains numerous sites at which isomorphous substitutions may occur. Piilonen *et al.* (2003) developed a standardized nomenclature and procedure for the calculation of the chemical formulae for minerals of the astrophyllite group. The general structural formula is:
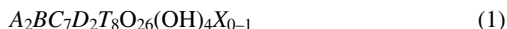
$$A_2BC_7D_2T_8O_{26}(OH)_4X_{0-1} \qquad (1)$$

where A = $^{[10]-[13]}$K, Rb, Cs, Na, H_3O^+, H_2O, or □; B = $^{[10]}$Na or Ca; C = $^{[6]}$Mn, Fe^{2+}, Fe^{3+}, Na, Mg, or Zn; D = $^{[6]}$Ti, Nb, or Zr; T = Si and Al, and X = F, OH, O, or □.

In this, the second part of an extensive study into the crystal chemistry of the astrophyllite group, we describe the structural, geometrical and stereochemical variations that result from chemical substitutions within the structure. This study is based on single-crystal X-ray refinements of the structure of 20 crystals of astrophyllite-group minerals from a variety of localities (Table 1), coupled with additional compositional data obtained by electron-microprobe analysis (EMPA), Fourier-transform infrared spectroscopy, and Mössbauer spectroscopy.

OVERVIEW OF THE HETEROPHYLLOSILICATE STRUCTURE

The crystal structure of magnesium astrophyllite was first determined by Peng & Ma (1963), and the structure of astrophyllite was determined by Woodrow (1967). Since then, structural studies of members of the astrophyllite group have been carried out on astrophyllite (Yamnova & Egorov-Tismenko 2000, Ma *et al.* 2000), magnesium astrophyllite (Shi *et al.* 1998), kupletskite (Christiansen *et al.* 1998, Piilonen *et al.* 2001), and niobokupletskite (Piilonen *et al.* 2000).

Ferraris *et al.* (1996), Ferraris (1997) and Christiansen *et al.* (1999) have described astrophyllite-group minerals and other modular titanosilicates, such as bafertisite (Pen & Sheng 1963), perraultite (Yamnova *et al.* 1998), nafertisite (Ferraris *et al.* 1996), lamprophyllite (Saf'yanov *et al.* 1983, Johnsen 1996), yoshimuraite (McDonald *et al.* 2000) and delindeite (Ferraris *et al.* 2001), as heterophyllosilicates. Such minerals have an *HOH* structure, reminiscent of the *TOT* structure in 2:1 phyllosilicates, where TiO_5 or TiO_6 polyhedra in the heterogeneous sheet (*H* sheet) proxy for the usual (Si,Al)O_4 tetrahedra in phyllosilicate *T*-sheets. Astrophyllite-group minerals can be considered as intermediate members in a polysomatic (Ferraris *et al.* 1996) or homologous (Christiansen *et al.* 1999) series that includes perraultite [KBaNa$_2$(Mn,Fe^{2+})$_8$ (Ti,Nb)$_4$Si$_8$O$_{32}$(OH,F,H$_2$O)$_7$] and trioctahedral micas as the end-member structures. A comparison of these minerals shows that they all have: (1) an *HOH* structure, (2) an a axial length of approximately 5.4 Å, corresponding to the a value in micas, and (3) $d_{001} \approx 10.9$ Å. Members of the homologous series can be classified by the number of diorthosilicate groups (n) separating rows of D octahedra: n = 1 in perraultite and bafertisite, n = 2 in astrophyllite-group minerals, n = 3 in nafertisite, and n = ∞ in micas (Ferraris *et al.* 1996, Christiansen *et al.* 1999).

In bafertisite, lamprophyllite and yoshimuraite, the *H* sheet is composed of $[Si_2O_7]^{6-}$ dimers linked *via* corner-sharing TiO_6 octahedra or TiO_5 tetragonal pyramids, resulting in a Si:Ti ratio of 2:1. The offset between successive *HOH* layers is such that the TiO_n polyhedra are not linked across the interlayer, as observed in astrophyllite-group minerals and nafertisite. In nafertisite, the *H*-layer consists of open-branched *zweier* [100] double chains of composition $[Si_{12}O_{34}]^{20-}$ (Liebau 1985) cross-linked by TiO_6 octahedra, which bridge across the interlayer, resulting in a Si:Ti ratio of 6:1 (Ferraris *et al.* 1996). The astrophyllite structure may be considered an intermediate member of the polysomatic series (n = 2).

In a general sense, the astrophyllite structure can be subdivided into two main composite sheets stacked along [001] in a 2:1 ratio. The first is a sheet of closest-packed MO_6 octahedra sandwiched between two *H*

sheets that are related by an inversion center in the triclinic species and by a two-fold axis parallel to b in kupletskite-$Ma2b2c$. The H sheet has the ideal composition $[DSi_4O_{12}]^{4-}$ and consists of open-branched *zweier* [100] single chains of composition $[Si_4O_{12}]^{8-}$ (Liebau 1985), which are cross-linked by corner-sharing $D\phi_6$ octahedra in triclinic species and kupletskite-$Ma2b2c$, and DO_5 polyhedra in magnesium astrophyllite (Shi *et al.* 1998). The resultant Si:D ratio is 4:1. Individual $D\phi_6$ octahedra are linked across the interlayer *via* a common apical anion, $\phi(16)$ (ϕ: unspecified ligand). The $\phi(16)$ anion is located at an inversion center in triclinic species, at the special position $4e$ in kupletskite-$Ma2b2c$, and is absent in magnesium astrophyllite (Shi *et al.* 1998). There is a misfit between the O and H sheets, similar to that observed in micas, which is compensated for by tilting and rotation of SiO_4 tetrahedra and distortion or corrugation of the O sheet. The degree to which this misfit occurs is dependent on the composition of the O sheet, decreasing with increasing size of the O-sheet cations (Woodrow 1967, Christiansen *et al.* 1998, Shi *et al.* 1998). The steric details of this misfit are discussed further below.

The interlayer of triclinic samples contains two crystallographically distinct and highly ordered sites: a 10-coordinated site (B) hosts Na and Ca, and a larger, [11]- to [13]-coordinated site (A) is dominated by K but commonly contains Rb, Cs, Ba, Na, and vacancies ($\square$). In monoclinic kupletskite-$Ma2b2c$, there are three distinct interlayer sites: $A(1)$, $A(2)$ and B. The stacking of HOH layers along [001] results in an excellent (001) cleavage, yet a slightly more brittle character than observed in other phyllosilicates owing to the existence of the bridging $\phi(16)$ anion within the interlayer. The crystal structures of triclinic astrophyllite-group minerals, monoclinic kupletskite and magnesium astrophyllite are shown in Figures 1A to C.

ANALYTICAL METHODS

Table 1 lists the provenance of each of the 20 samples studied. In all cases (except NOR17, the crystal for which was lost during transfer), chemical data were collected on the same crystal as that used for the single-crystal X-ray refinement. An attempt was made to cover the entire possible range in chemical variations observed in astrophyllite-group of minerals, with particular interest paid to variations in the proportions of alkalis (Na, K), [6]-coordinated cations [Mn, Fe, Mg, Zn in the O sheet and high-field-strength elements (Ti,

TABLE 1. LOCALITY INFORMATION FOR SINGLE CRYSTALS OF THE ASTROPHYLLITE GROUP

Code	Sample (Collection) #	Species	Locality and rock type
GJER			Gjerdingen intrusion, Norway
	NOR17 (LHN-5)	kupletskite	- alkali granite
KHIB			Khibina massif, Kola Peninsula, Russia
	RUS4 (CMNMI-53187)	astrophyllite	- nepheline syenite pegmatite
	RUS8 (FMM-1)	astrophyllite	- nepheline syenite pegmatite
LAB			Seal Lake, Labrador, Canada
	LAB3 (GSC-M26148-B)	astrophyllite	- peralkaline nepheline gneiss
LANG			Langesundsfjord area, Oslo Rift Valley, Norway
	NOR1 (RW-1)	astrophyllite	- nepheline syenite pegmatite (Vesle Arøya)
LOV			Lovozero massif, Kola Peninsula, Russia
	RUS9 (HC-1048)	kupletskite	- nepheline syenite pegmatite (Lephke-Nelm)
	RUS12 (FMM-56274)	kupletskite	- nepheline syenite pegmatite (Kukisvumchorr Mt.)
MSH			Mont Saint-Hilaire, Québec, Canada
	MSH2 (NMNS-4)	kupletskite	- nepheline syenite pegmatite
	MSH3 (NMNS-5)	kupletskite	- nepheline syenite pegmatite
	MSH8 (NMNS-12)	kupletskite	- altered nepheline syenite pegmatite
	MSH9 (NMNS-13)	kupletskite	- nepheline syenite pegmatite
	MSH15 (NMNS-22)	kupletskite	- nepheline syenite pegmatite
	MSH19A (NMNS-26)	kupletskite	- altered nepheline syenite pegmatite
	MSH20 (NMNS-27)	kupletskite	- nepheline syenite pegmatite
	MSH33A (CMNMC)	astrophyllite	- aplite/pegmatite
	MSH34A (CMNMC)	astrophyllite	- nepheline syenite pegmatite
	MSH38A (CMNMC)	kupletskite	- altered nepheline syenite pegmatite
	MSH42[*]	niobokupletskite	- nepheline syenite pegmatite
PP			Mount Rosa, Pikes Peak, Colorado, USA
	US5 (CMNMC)	astrophyllite	- granitic pegmatite

CMNMC/CMNMI/NMNS = Canadian Museum of Nature collection, GSC = Geological Survey of Canada collection, FMM = Fersman Mineralogical Museum collection, RW = R. Werner collection, HC/LHN = L. Horváth collection,
[*] Holotype niobokupletskite
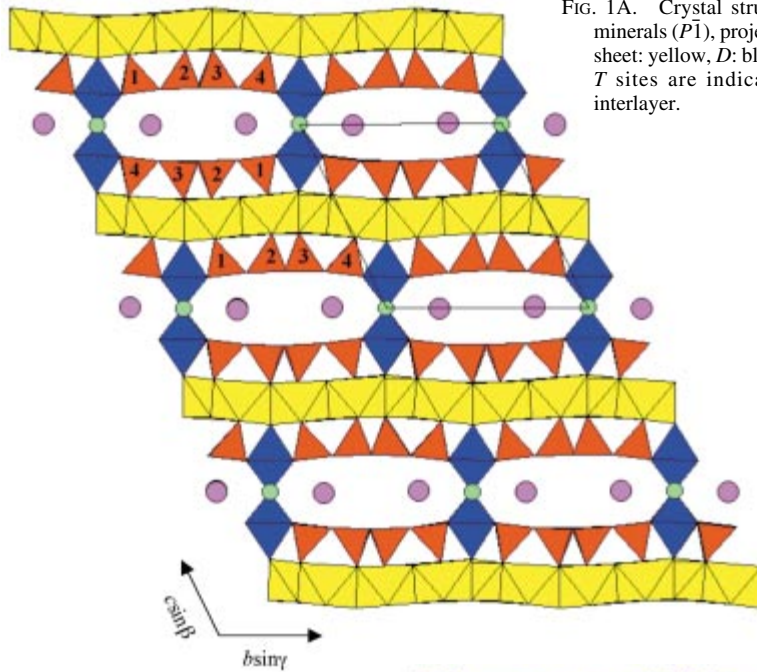
Fig. 1A. Crystal structure of triclinic astrophyllite-group minerals ($P\bar{1}$), projected down [100] (unit cell outlined). *O* sheet: yellow, *D*: blue, *T*: red, *A*: purple, *B*: green. The four *T* sites are indicated to show symmetry across the interlayer.

Fig. 1B. Crystal structure of kupletskite (monoclinic, *C*2/*c*), projected down [100] (unit cell outlined). *O* sheet: yellow, *D*: blue, *T*: red, K: purple, Na: green. The four *T* sites are indicated to show symmetry across the interlayer.
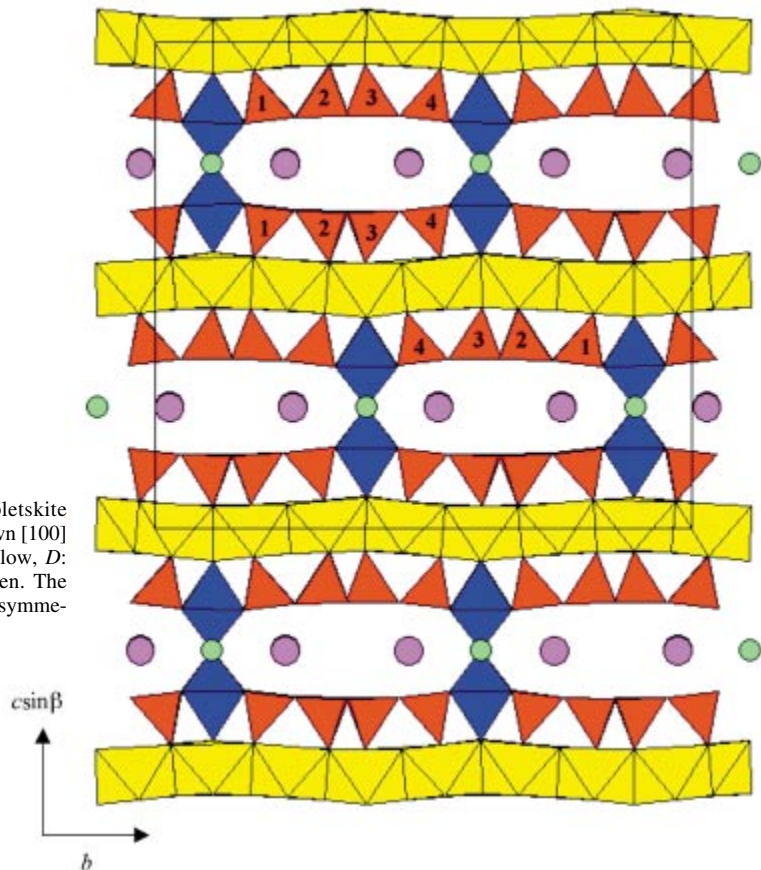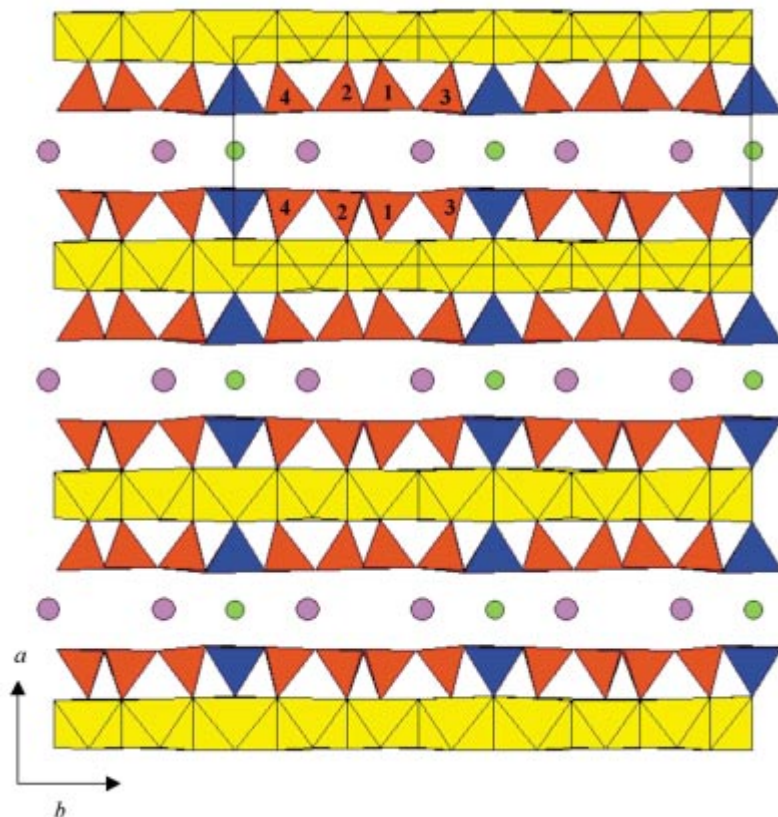
FIG. 1C. Crystal structure of magnesium astrophyllite (monoclinic, *A*2), projected down [001] (unit cell outlined). *O* sheet: yellow, *D*: blue, *T*: red, K: purple, Na: green. The four *T* sites are indicated to show symmetry across the interlayer. [Note: The atom coordinate given by Shi *et al.* (1998) for *z* of Si(2) is incorrect. The correct atom coordinate is $z = –0.0797$].

Zr, Nb) in *D*], and F. For a detailed explanation of the methods used for Fourier-transform infrared spectroscopy and Mössbauer spectroscopy, see Piilonen *et al.* (2003).

Electron-microprobe analyses

Electron-microprobe analyses (EMPA) were done with a JEOL 733 electron microprobe, operating in wavelength-dispersion mode, using Tracor Northern 5500 and 5600 automation. Details concerning operating conditions and selection of standards are given in Piilonen e*t al.* (2003). Table 2 contains average results for each single crystal, with chemical formulae calculated based on a total of 31 anions and 4(OH) + 1(F,O,OH) (Piilonen *et al.* 2003).

X-ray crystallography

Intensity data were collected on three different single-crystal X-ray diffractometers. All samples were hand-picked under the binocular microscope to ensure that they are free of macroscopic inclusions, and then observed under the polarizing microscope to check for optical continuity. Selected grains were also analyzed by the precession method to test for the presence of intergrowths and twinning.

Intensity data for six samples were collected using the Siemens SMART system at the University of Ottawa consisting of a three-circle goniometer and a 1 K (diameter: 9 cm, 512 × 512 pixel) CCD area-detector. Data were collected at room temperature using monochromatic Mo*K*α X-radiation (40 kV, 30 mA) and a fixed detector-to-crystal distance of 12.6 cm. Frame widths of 0.3° ω and count exposure-times of 30 s/frame were used. Data collection included unit-cell determi-

TABLE 2. ELECTRON-MICROPROBE DATA FOR SINGLE CRYSTALS OF ASTROPHYLLITE-GROUP MINERALS

Oxide	LAB 3	NOR 1	RUS 4	RUS 8	RUS 9	RUS 12	US 5	MSH 2	MSH 3
Na$_2$O wt.%	2.58	2.68	2.07	2.40	2.07	2.61	2.95	2.98	3.66
K$_2$O	5.81	5.21	6.02	6.21	6.21	5.91	5.45	5.61	5.46
Rb$_2$O	0.38	1.05	0.40	0.29	0.50	0.50	1.26	0.37	0.58
Cs$_2$O	0.06	1.35	0.03	0.00	0.03	0.00	0.09	0.00	0.00
CaO	0.64	1.00	1.59	1.60	1.27	1.38	0.08	0.75	0.03
SrO	0.20	0.10	0.39	0.25	0.27	0.23	0.01	0.05	0.10
BaO	0.00	0.00	0.20	0.23	0.52	0.07	0.19	0.20	0.00
MgO	0.65	1.11	1.66	1.71	1.42	1.94	1.94	0.44	0.44
MnO	14.19	13.99	11.04	12.30	21.46	27.53	4.80	30.81	26.26
FeO	19.49	18.45	21.80	20.00	10.98	4.13	27.59	2.00	0.13
ZnO	0.00	0.49	0.47	0.31	0.00	0.00	2.67	0.75	6.78
Al$_2$O$_3$	0.77	1.01	1.22	1.06	1.04	0.24	0.16	0.74	0.26
Y$_2$O$_3$	0.00	0.00	0.00	0.00	0.00	0.00	0.00	0.00	0.00
Ce$_2$O$_3$	0.17	0.31	0.11	0.00	0.29	0.07	0.17	0.54	0.00
TiO$_2$	6.59	9.20	11.41	11.20	10.52	11.40	9.28	10.80	7.05
SnO$_2$	0.00	0.23	0.00	0.00	0.00	0.00	0.60	0.00	0.00
ZrO$_2$	6.25	1.69	0.57	0.61	0.00	0.00	0.76	0.00	0.00
HfO$_2$	0.00	0.00	0.00	0.00	0.00	0.00	0.00	0.00	0.00
Nb$_2$O$_5$	1.60	2.81	0.89	0.59	2.38	0.77	3.07	1.91	7.81
Ta$_2$O$_5$	0.00	0.00	0.15	0.00	0.00	0.00	0.18	0.00	0.00
SiO$_2$	33.63	33.98	34.85	34.55	34.64	36.35	34.45	34.29	34.60
F	1.15	1.38	1.05	0.94	1.16	1.16	1.24	1.31	0.70
H$_2$O	2.69	2.65	2.90	2.90	2.83	2.85	2.68	2.67	2.60
O=F	-0.48	-0.58	-0.44	-0.40	-0.46	-0.49	-0.52	-0.55	-0.29
Total	96.35	98.12	98.34	96.77	97.02	96.68	97.14	95.67	96.11

Formula based on 31 anions

	LAB 3	NOR 1	RUS 4	RUS 8	RUS 9	RUS 12	US 5	MSH 2	MSH 3
K *apfu*	1.72	1.51	1.70	1.77	1.77	1.67	1.60	1.63	1.61
Rb	0.06	0.15	0.06	0.04	0.07	0.07	0.19	0.05	0.09
Cs	0.01	0.13	0.00	0.00	0.00	0.00	0.01	0.00	0.00
Sr	0.03	0.01	0.05	0.03	0.03	0.03	0.00	0.01	0.01
Ba	0.00	0.00	0.02	0.02	0.05	0.01	0.02	0.02	0.00
Na	0.12	0.09	0.00	0.12	0.00	0.02	0.03	0.15	0.12
ΣA	1.81	1.80	1.82	1.87	1.93	1.79	1.81	1.71	1.71
Na	0.84	0.76	0.61	0.62	0.52	0.65	0.98	0.82	0.99
Ca	0.16	0.24	0.38	0.38	0.31	0.33	0.02	0.18	0.01
ΣB	1.00	1.00	0.99	1.00	0.82	0.97	1.00	1.00	1.00
Na	0.20	0.33	0.28	0.30	0.38	0.44	0.30	0.35	0.53
Mg	0.22	0.38	0.55	0.57	0.47	0.64	0.00	0.15	0.15
Mn	2.79	2.69	2.07	2.33	4.07	5.15	0.93	5.95	5.14
Fe^{2+}	3.78	3.50	4.02	3.74	2.06	0.77	5.30	0.38	0.02
Zn	0.00	0.08	0.08	0.05	0.00	0.00	0.45	0.13	1.16
Y	0.00	0.00	0.00	0.00	0.00	0.00	0.00	0.00	0.00
Ce	0.01	0.03	0.01	0.00	0.02	0.01	0.02	0.05	0.00
ΣC	7.00	7.00	7.00	7.00	7.00	7.00	7.00	7.00	7.00
Ti	1.15	1.57	1.89	1.89	1.78	1.90	1.60	1.85	1.23
Sn	0.00	0.02	0.00	0.00	0.00	0.00	0.06	0.00	0.00
Zr	0.71	0.19	0.06	0.07	0.00	0.00	0.09	0.00	0.00
Hf	0.00	0.00	0.00	0.00	0.00	0.00	0.00	0.00	0.00
Nb	0.17	0.29	0.09	0.06	0.24	0.08	0.32	0.20	0.82
Ta	0.00	0.00	0.01	0.00	0.00	0.00	0.01	0.00	0.00
ΣD	2.02	2.06	2.05	2.01	2.02	1.97	2.07	2.05	2.04
Si	7.80	7.70	7.69	7.73	7.76	8.03	7.91	7.81	8.00
Al	0.21	0.27	0.32	0.28	0.28	0.06	0.04	0.20	0.07
ΣT	8.01	7.97	8.01	8.01	8.04	8.09	7.96	8.01	8.07
F	0.84	0.99	0.73	0.67	0.78	0.81	0.90	0.94	0.51
OH	4.16	4.01	4.27	4.33	4.23	4.20	4.10	4.06	4.00
O	30.16	30.01	30.27	30.33	26.00	26.00	30.10	30.06	30.49
Σcat.	19.96	19.93	19.86	20.01	19.80	19.83	19.87	19.92	19.93

Oxide	MSH 8	MSH 9	MSH 15	MSH 15A	MSH 19A	MSH 20	MSH 33A	MSH 34	MSH 38A	MSH 42
Na$_2$O	3.04	2.62	3.12	3.38	2.65	2.82	2.37	2.33	2.44	2.62
K$_2$O	6.30	5.49	5.52	5.59	5.86	5.60	6.04	6.04	5.64	5.97
Rb$_2$O	0.51	0.46	0.58	0.58	0.38	0.74	0.40	0.35	0.44	0.82
Cs$_2$O	0.00	0.00	0.00	0.06	0.00	0.06	0.06	0.07	0.00	0.12
CaO	0.44	0.78	0.20	0.13	0.22	1.12	0.56	0.93	0.81	0.00
SrO	0.00	0.09	0.28	0.05	0.03	0.06	0.20	0.26	0.03	0.00
BaO	0.00	0.18	0.09	0.00	0.00	0.25	0.00	0.00	0.00	0.00
MgO	0.51	0.43	1.05	0.98	0.53	0.53	0.56	0.50	0.47	0.15
MnO	23.54	29.99	26.71	21.64	19.34	28.65	14.56	8.95	17.98	26.37
FeO	9.66	1.91	6.19	10.00	13.39	1.02	18.95	24.96	14.85	2.64
ZnO	0.64	0.67	0.00	0.26	0.28	4.45	0.00	0.00	0.22	4.08
Al$_2$O$_3$	0.96	0.86	0.40	0.63	0.43	0.70	1.29	1.32	0.58	1.14
Y$_2$O$_3$	0.00	0.00	0.00	0.00	0.00	0.00	0.00	0.00	0.00	0.00
Ce$_2$O$_3$	0.00	0.58	0.08	0.00	0.00	0.34	0.26	0.00	0.15	0.00
TiO$_2$	6.20	10.28	8.29	6.84	6.89	11.25	5.43	7.31	9.01	1.34
SnO$_2$	0.00	0.00	0.00	0.00	0.00	0.00	0.00	0.00	0.00	0.00
ZrO$_2$	0.38	0.00	0.10	0.50	1.92	0.00	6.30	4.36	0.49	3.43
HfO$_2$	0.00	0.00	0.00	0.00	0.00	0.00	0.08	0.00	0.00	0.00
Nb$_2$O$_5$	8.59	1.93	6.06	7.51	5.05	0.96	3.46	2.80	3.52	12.13
Ta$_2$O$_5$	0.00	0.00	0.00	0.00	0.00	0.00	0.00	0.16	0.00	0.63
SiO$_2$	34.62	35.35	35.31	34.24	34.79	34.46	32.63	33.09	35.00	31.85
F	0.87	1.09	0.91	1.00	1.01	1.19	1.08	1.20	0.91	0.14
H$_2$O	2.93	2.63	2.67	2.80	2.77	2.73	2.70	2.68	2.61	2.48
O=F	-0.37	-0.46	-0.38	-0.42	-0.43	-0.50	-0.45	-0.51	-0.38	-0.06
Total	98.83	94.88	97.12	95.77	95.12	96.44	96.48	96.81	94.76	95.85

Formula based on 31 anions

	MSH 8	MSH 9	MSH 15	MSH 15A	MSH 19A	MSH 20	MSH 33A	MSH 34	MSH 38A	MSH 42
K *apfu*	1.80	1.60	1.59	1.63	1.73	1.62	1.80	1.78	1.66	1.84
Rb	0.07	0.07	0.08	0.09	0.06	0.11	0.06	0.05	0.07	0.13
Cs	0.00	0.00	0.00	0.01	0.00	0.01	0.01	0.01	0.00	0.01
Sr	0.00	0.01	0.04	0.01	0.00	0.01	0.03	·0.04	0.00	0.00
Ba	0.00	0.02	0.01	0.00	0.00	0.02	0.00	0.00	0.00	0.00
Na	0.01	0.00	0.03	0.03	0.00	0.18	0.02	0.00	0.00	0.00
ΣA	1.87	1.69	1.71	1.73	1.79	1.77	1.89	1.87	1.72	1.98
Na	0.87	0.62	0.95	0.97	0.78	0.73	0.86	0.77	0.66	0.95
Ca	0.11	0.19	0.05	0.03	0.05	0.27	0.14	0.23	0.20	0.00
ΣB	0.98	0.81	1.00	1.00	0.83	1.00	1.00	1.00	0.86	0.95
Na	0.45	0.54	0.38	0.51	0.41	0.34	0.20	0.27	0.43	0.28
Mg	0.17	0.15	0.35	0.34	0.18	0.18	0.20	0.17	0.16	0.05
Mn	4.47	5.79	5.10	4.20	3.78	5.51	2.88	1.75	3.50	5.40
Fe^{2+}	1.81	0.36	1.17	1.92	2.58	0.19	3.70	4.81	2.86	0.53
Zn	0.11	0.11	0.00	0.04	0.05	0.75	0.00	0.00	0.04	0.73
Y	0.00	0.00	0.00	0.00	0.00	0.00	0.00	0.00	0.00	0.00
Ce	0.00	0.05	0.01	0.00	0.00	0.03	0.02	0.00	0.01	0.00
ΣC	7.00	7.00	7.00	7.00	7.00	7.00	7.00	7.00	7.00	7.00
Ti	1.05	1.76	1.40	1.18	1.20	1.92	0.95	1.27	1.56	0.24
Sn	0.00	0.00	0.00	0.00	0.00	0.00	0.00	0.00	0.00	0.00
Zr	0.04	0.00	0.01	0.06	0.22	0.00	0.72	0.49	0.06	0.41
Hf	0.00	0.00	0.00	0.00	0.00	0.00	0.01	0.00	0.00	0.00
Nb	0.87	0.20	0.62	0.78	0.53	0.10	0.37	0.29	0.37	1.33
Ta	0.00	0.00	0.00	0.00	0.00	0.00	0.00	0.01	0.00	0.04
ΣD	1.96	1.96	2.03	2.01	1.94	2.02	2.04	2.06	1.98	2.02
Si	7.76	8.06	7.96	7.84	8.03	7.83	7.62	7.63	8.05	7.71
Al	0.25	0.23	0.10	0.17	0.12	0.19	0.36	0.36	0.16	0.33
ΣT	8.01	8.29	8.06	8.01	8.14	8.02	7.98	7.99	8.21	8.03
F	0.62	0.79	0.64	0.73	0.74	0.86	0.80	0.88	0.66	0.11
OH	4.38	4.00	4.00	4.28	4.26	4.15	4.20	4.13	4.00	4.00
O	30.38	30.21	30.36	30.28	30.26	30.15	30.20	30.13	30.34	30.89
Σcat.	19.82	19.76	19.84	19.78	19.70	19.98	19.93	19.92	19.77	19.98

nation (~18 minutes) and collection of all data frames (17.5 hours). The data were reduced, filtered, integrated, and corrected for Lorentz, polarization and background effects using the Siemens software SAINT. Psi-scan absorption corrections were performed using the Siemens program XPREP (Bruker 1997), during which the crystals were modeled as {001} plates. A range of plate-glancing angles was tested for each crystal (generally 2–9°), with the angle yielding the best transmission factors chosen for the absorption correction.

Intensity data for 11 samples were collected using the Siemens SMART system at the University of Manitoba, consisting of a four-circle goniometer and a 1 K (diameter: 9 cm, 512 × 512 pixel) CCD area-detector. Data were collected at room temperature using monochromatic MoKα X-radiation (50 kV and 40 mA) and a fixed detector-to-crystal distance of 4 cm. Frame widths of 0.2° ω and count exposure-times of 45 s were used. Data collection consisted of 4349 frames, to 60° 2θ, which provided 100% coverage of the diffraction sphere, with a mean redundancy of 3.6. Approximately 1000 reflections with spot sizes of 2.4° (within the plane) and 2.0° (normal to the plane) were used in the determination of each orientation matrix, and a preliminary unit-cell prior to integration of all data frames. Data integration was done using the Siemens software SAINT. Absorption corrections were done using SADABS, and crystals were modeled as ellipses. All reflection data were then merged using the program XPREP (Bruker 1997).

X-ray intensity data for two samples were collected on a Siemens $P3$ four-circle diffractometer at the University of Manitoba, operating at 50 kV and 40 mA, equipped with a standard serial detector. Each orientation matrix was obtained by collecting intensity data for 50 random reflections within the range 12 to 35° 2θ. Following determination of the orientation matrix, half a sphere of intensity data was collected in the range of 4 to 60° 2θ using scan speeds inversely proportional to peak intensity (range: 3 to 29.3° 2θ/min) and scan range of ±1.3° 2θ about the peak centroid. In order to monitor experimental conditions over time, the intensity of one standard reflection ($\bar{1}\bar{3}0$) was collected every 50 reflections; no significant variations were observed.

The structure of 19 triclinic samples was refined in space group $P\bar{1}$ by least-squares methods using the SHELXL–93 set of programs (Sheldrick 1993), whereas the structure of monoclinic kupletskite was solved and refined in space group $C2/c$. All atom coordinates and temperature factors were kept as refineable parameters during the refinement process. Except for cases in which the interlayer site A was split owing to positional disorder, all displacement parameters were refined on an anisotropic basis. Site-occupancy factors (SOF) for all anions were fixed at unity. During the initial refinement, cation assignments to the A, B, $M(1)$ through $M(4)$, and D sites were made on the basis of the compositional data obtained from EMPA. Scattering curves for neutral at-

oms were those of Cromer & Liberman (1970). In cases where the site-scattering refinements (SREF) indicated the presence of a second scattering species, the two predominant elements (on the basis of EMPA), were assigned to that site, and the SOF was constrained to be unity. Secondary isotropic-extinction corrections applied to all datasets did not improve the results.

Unit-cell parameters and information pertinent to the data collection and crystal-structure refinement are shown in Table 3. Final positional and anisotropic displacement parameters and complete bond-valence tables can be obtained from the Depository of Unpublished Data, CISTI, National Research Council of Canada, Ottawa, Ontario K1A 0S2, Canada. Selected bond-lengths are given in Table 4.

The description of the structure of a crystal would not be complete without the detailed analysis of the geometry of individual polyhedra and its variation in response to cation and anion substitutions. Although determination of the coordination number, bond lengths and bond angles of polyhedra within the astrophyllite group is straightforward, the majority of polyhedra within the H and O sheets display marked departures from regularity and an ideal geometry. In order to describe these irregularities, we must compare refined parameters to those predicted for ideal or model polyhedra. Parameters commonly used to quantify distortions in coordination polyhedra include quadratic elongation (Robinson *et al.* 1971), normalized bond-length variations (Brown & Shannon 1973, Shannon 1975, 1976), octahedron flattening (Weiss *et al.* 1985), and centroid and sphericity determination (Balić-Žunić & Makovicky 1996, Makovicky & Balić-Žunić 1998).

The normalized bond-length variation or distortion (Δ) of the polyhedra in the H and O sheets was calculated using the equation:

$$\Delta \equiv \left\{ \sum_{i=1}^{n} \left[\left(l_i - l_m \right)^2 / n \right]^2 / n \right\} \cdot 10^4 \qquad (2)$$

(Brown & Shannon 1973, Shannon 1975, 1976) where l_i = bond length, l_m = mean bond-length, and n = coordination number. The tetrahedral- and octahedral-angle variance (TAV and OAV, respectively), an alternative measure of polyhedron distortion, can be calculated using the equations developed by Robinson *et al.* (1971):

$$\text{TAV} = \sigma_T^2 = \sum_{i=1}^{6} \left[(O - T - O) - 109.47 \right]^2 / 5 \qquad (3)$$

$$\text{OAV} = \sigma_M^2 = \sum_{i=1}^{12} \left[(O - T - O) - 90 \right]^2 / 11 \qquad (4).$$

TABLE 3. UNIT-CELL DIMENSIONS AND STRUCTURE-REFINEMENT DATA FOR ASTROPHYLLITE-GROUP MINERALS

Sample	S.G.	a	b	c	V	α	β	γ	E^2-1	CFOM	N/N$_u$	N$_i$	$R1$	$wR2$	GooF
LAB3	$P\bar{1}$	5.4049(3)	11.9175(6)	11.7488(6)	666.5(1)	112.93(1)	94.627(1)	103.139(1)	1.038	1.46	6942/3870	7	6.21	8.97	0.928
NOR1	$P\bar{1}$	5.3857(3)	11.9072(7)	11.7105(7)	660.9(1)	113.062(1)	94.614(1)	103.098(1)	1.053	2.08	6883/3836	3	9.12	11.71	0.916
NOR17	$P\bar{1}$	5.3784(2)	11.9085(5)	11.7236(4)	661.09(7)	112.964(1)	94.697(1)	103.112(1)	1.075	1.9	6855/3835	8	6.05	12.69	1.044
RUS4	$P\bar{1}$	5.3776(6)	11.899(1)	11.662(1)	656.2(2)	113.114(2)	94.630(2)	103.090(2)	1.113	2.73	3377/2532	25	6.12	14.66	1.183
RUS8	$P\bar{1}$	5.3754(3)	11.8970(6)	11.6634(6)	655.99(6)	113.133(4)	94.638(4)	103.081(4)	1.123	2.89	3571/3421	0	3.38	7.76	1.053
RUS9	$C2/c$	5.4022(2)	23.226(1)	21.1782(9)	2646.2(3)	90	95.246(1)	90	1.294	11.02	13834/3865	2	8.42	14.04	0.945
RUS12	$P\bar{1}$	5.3925(2)	11.9283(4)	11.7256(4)	663.39(7)	113.044(1)	94.840(1)	103.064(1)	1.081	1.94	6813/3834	17	5.51	11.25	1.082
US5	$P\bar{1}$	5.3627(8)	11.851(2)	11.668(2)	652.9(3)	113.040(3)	94.523(2)	103.093(2)	1.138	3.85	3715/2669	12	7.21	15.23	1.056
MSH2	$P\bar{1}$	5.3982(2)	11.9534(4)	11.7433(4)	666.79(6)	112.9903(8)	94.8413(7)	103.0664(8)	1.081	1.73	6877/3853	49	4.69	11.75	1.084
MSH3	$P\bar{1}$	5.3887(8)	11.913(2)	11.751(2)	664.0(3)	112.961(4)	94.746(3)	103.117(3)	1.028	1.32	3917/2831	25	7.06	11.51	1.107
MSH8	$P\bar{1}$	5.4203(2)	11.9392(4)	11.7229(4)	667.42(7)	113.0010(7)	94.7348(9)	103.1598(9)	1.027	1.09	6910/3860	15	4.90	9.01	0.974
MSH9	$P\bar{1}$	5.3989(3)	11.9528(7)	11.7458(7)	667.0(1)	112.983(1)	94.854(1)	103.062(1)	1.076	2.46	6940/3863	1	8.30	9.89	0.916
MSH15	$P\bar{1}$	5.4033(6)	11.920(1)	11.741(1)	665.7(2)	112.933(3)	94.793(2)	103.108(2)	1.031	1.01	3641/2669	22	5.57	16.58	1.091
MSH15A	$P\bar{1}$	5.4039(2)	11.9243(4)	11.7394(4)	665.94(7)	112.942(1)	94.732(1)	103.135(1)	1.015	0.76	6892/3860	23	4.56	10.52	1.07
MSH19A	$P\bar{1}$	5.4206(2)	11.9283(5)	11.7294(5)	667.46(8)	112.942(1)	94.645(1)	103.246(1)	1.066	1.75	6949/3869	21	5.93	10.71	0.998
MSH20	$P\bar{1}$	5.3879(3)	11.9263(7)	11.7136(6)	661.98(6)	113.049(4)	94.832(4)	103.077(4)	1.112	2.67	3584/3443	0	3.97	8.34	1.078
MSH33A	$P\bar{1}$	5.418(1)	11.933(2)	11.742(2)	668.5(4)	112.962(3)	94.620(3)	103.123(4)	1.062	1.72	3945/2871	26	6.25	13.61	1.13
MSH34A	$P\bar{1}$	5.3996(2)	11.9152(4)	11.7077(4)	663.00(6)	113.0413(7)	94.5707(7)	103.1239(8)	1.086	1.98	6895/3842	28	4.59	10.10	1.025
MSH38A	$P\bar{1}$	5.4028(2)	11.9178(4)	11.7000(4)	662.73(7)	113.036(1)	94.671(1)	103.163(1)	1.061	1.45	68543826	27	4.43	9.61	1.054
MSH42	$P\bar{1}$	5.4303(9)	11.924(2)	11.747(2)	669.5(3)	112.927(3)	94.750(3)	103.175(3)	0.985	1.08	5219/3023	77	5.97	10.23	1.085

S.G.: space group, N: total number of reflections collected, N$_u$: number of unique reflections, N$_i$: inconsistent reflections, GooF: goodness-of-fit, E^2-1: normalized structure-factor, CFOM: combined figure of merit. The unit-cell dimensions a, b and c are expressed in Å, the volume, in Å^3, and the interaxial angles, in degrees. The residuals $R1$ and $wR2$ are expressed as percentages.

The octahedron flattening angle (Ψ) is defined as the angle between the normal to the upper or lower trigonal faces and the average diagonal length. Values of Ψ were calculated using the program OCTAHEDRON (Evans 2000). Given the coordinates of the points of an MO_6 octahedron ($\mathbf{r}_i = r_i, \theta_i, \phi_i$), the M–O bond length, angle of flattening, (Ψ), and the counter-rotation angle (δ) can easily be found. A least-squares method is used to fit the coordinates to an octahedron where flattening and counter-rotation are the only distortions from octahedral symmetry. If $\{\mathbf{r}_1, \mathbf{r}_2, \mathbf{r}_3\}$ form the top face and $\{\mathbf{r}_4, \mathbf{r}_5, \mathbf{r}_6\}$ form the bottom face, this procedure gives:

$$\Psi = \frac{1}{6}\sum_{i=1}^{3}\phi_i - \frac{1}{6}\sum_{i=4}^{6}\phi_i + \frac{\pi}{2} \text{ and}$$

$$\delta = -\frac{1}{6}\sum_{i=1}^{3}\theta_i + \frac{1}{6}\sum_{i=4}^{6}\theta_i + \frac{\pi}{6} \qquad (5).$$

The thickening angle of a tetrahedron (τ), ideally 109.47° for an undistorted tetrahedron, was calculated as:

$$\tau_T = \sum_{i=1}^{3}\left(O_{basal} - T - O_{apical}\right)/3 \qquad (6).$$

Polyhedron volumes and tilt angles of tetrahedra [with respect to the (001) plane] were calculated using the program IVTON (Balić-Žunić & Vicković 1996). The rotation angle of the tetrahedra (α) was calculated using the following formula assuming an ideal O_{br}–O_{br}–O_{br} angle (O_{br}: bridging oxygen) of 120°:

$$\alpha = \frac{1}{2}|120 - <O_{br}-O_{br}-O_{br}>| \qquad (7).$$

Geometrical parameters for each of the polyhedra in the structures can be found in Table 5.

SITE-ASSIGNMENT PROCEDURE

Table 6 lists bond-valence sums (BVS; calculated using parameters taken from Brese & O'Keeffe 1991) and site-occupancy factors (SOF) for the refined cation sites. Unambiguous assignment of cations to the multiple sites in the astrophyllite structure requires a single-crystal X-ray refinement and detailed EMPA. Correct site-assignments are further complicated by the presence of vacancies and H_2O, by varying degrees of order within the O sheet, and by the presence of cations such as Na occupying sites within both the O sheet and the interlayer. Details of the site-assignment procedure followed during structure analysis are presented below.

The dominant interlayer cation at A in all astrophyllite-group minerals from this study was found to be K. In a number of triclinic structures, refinement of A =

K alone resulted in exceptionally large U_{11} anisotropic displacement factors, coupled with a large positive residual in the difference Fourier map (>2.5 e^{-1}). In samples where refinement of the SOF indicated the presence of a lighter X-ray scatterer, Na was assigned to *A*. Similarly, where SOF refinement indicated the presence of a heavier X-ray scatterer, Rb was assigned to *A* at the EMPA-established value, and the SOF was refined. In samples where the shape of the anisotropic displacement ellipsoid (of the site to which K was assigned) suggested positional disorder, refinement of the site occupancies failed to improve the displacement factors. The scattering was therefore modeled as two split sites, K(1a) and K(1b). In these cases, displacement factors for K(1a) and K(1b) were constrained to be equal and refined isotropically.

Sodium was assigned to *B* in all samples. Calcium was later included in the refinement where the SOF for *B* indicated the presence of a heavier X-ray scatterer than Na alone. Refined occupancies of Ca correlate well with values obtained from electron-microprobe data (Fig. 2).

Manganese and Fe were initially assigned to *M*(1) through *M*(4), depending on which cation was indicated to be dominant at *C*. The site-scattering refinement (SREF) for *M*(1) consistently yielded occupancies less than unity (20–30 standard deviations low), indicating the presence of a weaker X-ray scatterer. Electron-microprobe data indicate an excess of Na in the majority of samples if compared to results obtained from SREF of only *A* and *B*. The occupancy of *M*(1) was therefore

refined on the basis of (Mn + Fe + Na). A plot of the total SREF content of Na *versus* total Na as determined by EMPA (Fig. 3) indicates good agreement between the two methods. The presence of up to 0.274 *apfu* Na at *M*(1) site is not uncommon in astrophyllite-group minerals. For example, magnesium astrophyllite (Shi *et al.* 1998) exhibits a dominance of Na within a single octahedrally coordinated site equivalent to *M*(1) in triclinic samples and kupletskite-*Ma2b2c*. Substitution of Na for Mn in octahedral coordination, although generally uncommon owing to the 23% difference in ionic radii between the two cations, has also been noted in other minerals, including samuelsonite (Moore & Araki 1977), barytolamprophyllite (Rastsvetaeva & Dorfman 1995), vuonnemite (Ercit *et al.* 1998), delindeite (Ferraris *et al.* 2001), alkali clinoamphiboles from Mont Saint-Hilaire (MSH; Taylor 1999), and eudialyte-group minerals from MSH (Johnsen & Grice 1999). It is interesting to note that all these minerals crystallize in peralkaline environments where the activity of Na is high.

Site-scattering refinements for *M*(2), *M*(3) and *M*(4) generally yield occupancies close to unity, with slight departures from ideal being attributed to Mn ⇔ Fe substitution. In samples where site-scattering refinements indicated significant departures from the ideal (Fe,Mn) occupancies (*i.e.*, >10%) and the presence of a lighter or heavier X-ray scatterer, Mg or Zn were assigned to the site, with the total SOF constrained to be unity.

With the exception of niobokupletskite, all samples were found to be Ti-dominant in *D*. In samples where
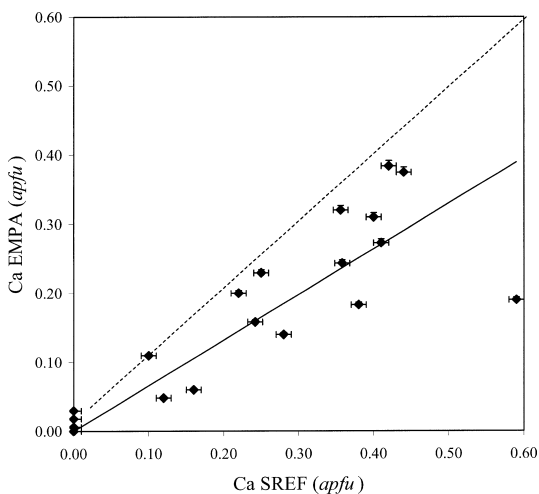
FIG. 2. Comparison of site refinement and electron-microprobe data: Ca SREF *versus* Ca EMPA (*apfu*). The 1:1 substitution line is indicated (dashed). The solid line represents the best-fit linear regression, with $y = 0.6596x$, $R^2 = 0.688$. Analytical errors are indicated.
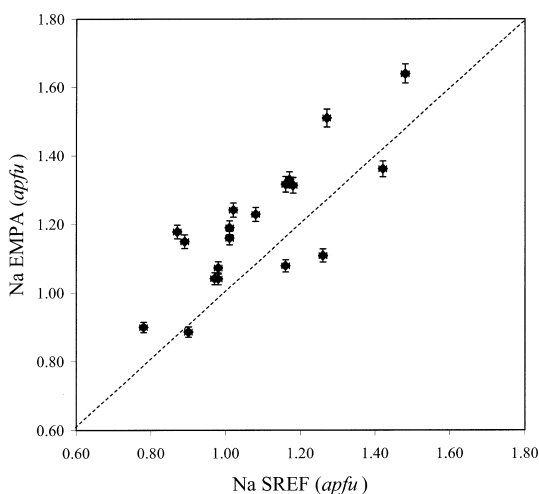
FIG. 3. Comparison of site refinement and electron-microprobe data: Na_{tot} SREF *versus* Na_{tot} EMPA (*apfu*). The 1:1 substitution line is indicated as a dashed line. Analytical errors are indicated.

TABLE 4. SELECTED BOND LENGTHS (Å) FOR ASTROPHYLLITE GROUP MINERALS

SAMPLE	LAB3	NOR1	NOR17	RUS4	RUS8	RUS9	RUS12	US5	MSH2	MSH3	MSH8	MSH9	MSH15	MSH15A	MSH19A	MSH20	MSH33A	MSH34	MSH38A	MSH42
$M(1)O_5(OH)$ octahedron																				
M(1)-O(2)	2.146(3)	2.170(3)	2.172(3)	2.163(5)	2.168(2)	2.178(3)	2.189(2)	2.137(5)	2.188(2)	2.187(4)	2.183(2)	2.188(3)	2.186(5)	2.180(2)	2.169(3)	2.187(2)	2.139(5)	2.142(2)	2.169(2)	2.179(8)
M(1)-O(5)	2.177(3)	2.174(4)	2.185(3)	2.175(5)	2.179(2)	2.187(4)	2.198(3)	2.156(5)	2.193(2)	2.212(5)	2.190(2)	2.192(3)	2.197(4)	2.192(2)	2.185(3)	2.191(2)	2.188(4)	2.166(2)	2.184(2)	2.194(8)
M(1)-O(6)	2.154(3)	2.162(3)	2.182(3)	2.158(5)	2.158(2)	2.172(3)	2.191(2)	2.147(5)	2.181(2)	2.192(4)	2.182(2)	2.185(3)	2.189(4)	2.190(2)	2.175(3)	2.180(2)	2.142(4)	2.143(2)	2.172(2)	2.190(7)
M(1)-O(3)	2.190(2)	2.190(4)	2.202(3)	2.185(5)	2.190(2)	2.199(4)	2.216(2)	2.172(5)	2.206(2)	2.218(4)	2.207(2)	2.204(3)	2.207(5)	2.208(2)	2.197(2)	2.206(2)	2.189(4)	2.177(2)	2.199(2)	2.209(7)
M(1)-O(7)	2.208(2)	2.204(4)	2.195(3)	2.206(5)	2.199(2)	2.213(4)	2.214(2)	2.174(5)	2.207(2)	2.221(4)	2.223(2)	2.209(3)	2.226(5)	2.215(2)	2.216(3)	2.209(2)	2.225(4)	2.202(2)	2.207(2)	2.221(7)
M(1)-O(1)	2.232(3)	2.231(4)	2.225(3)	2.223(4)	2.221(2)	2.234(4)	2.244(2)	2.205(5)	2.230(2)	2.244(4)	2.240(2)	2.230(3)	2.233(4)	2.239(2)	2.237(3)	2.231(2)	2.236(4)	2.226(2)	2.229(2)	2.247(7)
<M(1)-O>	2.185	2.189	2.194	2.185	2.186	2.197	2.209	2.165	2.201	2.212	2.204	2.201	2.206	2.204	2.196	2.201	2.187	2.176	2.193	2.207
$M(2)O_4(OH)_2$ octahedron																				
M(2)-O(7)	2.111(3)	2.105(3)	2.113(3)	2.085(5)	2.095(2)	2.118(3)	2.128(2)	2.087(5)	2.129(2)	2.121(4)	2.124(2)	2.130(3)	2.113(4)	2.122(2)	2.119(3)	2.123(2)	2.121(4)	2.103(2)	2.110(2)	2.133(8)
M(2)-O(5)	2.111(3)	2.106(4)	2.111(3)	2.093(5)	2.097(2)	2.112(3)	2.130(2)	2.079(5)	2.132(2)	2.131(4)	2.115(2)	2.139(3)	2.118(5)	2.119(2)	2.112(3)	2.131(2)	2.107(5)	2.096(2)	2.111(2)	2.124(7)
M(2)-O(5)	2.132(3)	2.135(4)	2.141(3)	2.128(5)	2.131(2)	2.149(4)	2.144(2)	2.116(5)	2.150(2)	2.139(4)	2.146(2)	2.149(3)	2.157(5)	2.146(2)	2.140(3)	2.142(2)	2.149(5)	2.130(2)	2.142(2)	2.152(8)
M(2)-O(6)	2.205(3)	2.195(4)	2.211(3)	2.192(5)	2.192(2)	2.207(4)	2.222(2)	2.199(5)	2.217(2)	2.214(4)	2.217(2)	2.223(3)	2.217(5)	2.213(2)	2.218(2)	2.216(2)	2.210(4)	2.192(2)	2.212(2)	2.211(7)
M(2)-O(7)	2.216(3)	2.216(3)	2.219(3)	2.210(5)	2.210(2)	2.224(4)	2.231(2)	2.208(5)	2.240(2)	2.226(4)	2.232(2)	2.236(3)	2.228(4)	2.224(2)	2.231(3)	2.229(2)	2.220(4)	2.213(2)	2.222(2)	2.254(7)
M(2)-O(2)	2.230(3)	2.248(4)	2.253(3)	2.247(5)	2.247(2)	2.252(4)	2.254(3)	2.233(5)	2.267(2)	2.262(4)	2.253(2)	2.261(3)	2.258(4)	2.255(2)	2.244(3)	2.263(2)	2.230(4)	2.238(2)	2.246(2)	2.252(8)
<M(2)-O>	2.168	2.168	2.175	2.159	2.162	2.177	2.185	2.154	2.189	2.182	2.181	2.190	2.182	2.180	2.177	2.184	2.173	2.162	2.174	2.188
$M(3)O_4(OH)_2$ octahedron																				
M(3)-O(1)	2.128(2)	2.112(3)	2.126(3)	2.112(5)	2.108(2)	2.127(3)	2.135(2)	2.098(5)	2.138(2)	2.127(4)	2.138(2)	2.139(3)	2.130(4)	2.136(2)	2.135(4)	2.135(2)	2.129(4)	2.119(2)	2.125(2)	2.143(7)
M(3)-O(4)	2.117(3)	2.129(4)	2.125(3)	2.110(5)	2.113(2)	2.124(4)	2.137(3)	2.107(5)	2.143(2)	2.134(4)	2.133(2)	2.146(3)	2.132(4)	2.130(2)	2.122(3)	2.137(2)	2.117(5)	2.112(2)	2.122(2)	2.145(7)
M(3)-O(3)	2.138(3)	2.133(3)	2.137(3)	2.109(5)	2.120(2)	2.140(3)	2.153(2)	2.115(5)	2.156(2)	2.148(4)	2.149(2)	2.158(3)	2.159(4)	2.147(2)	2.149(5)	2.152(2)	2.133(4)	2.125(2)	2.140(2)	2.151(7)
M(3)-O(6)	2.152(3)	2.149(4)	2.157(3)	2.141(4)	2.137(2)	2.158(4)	2.170(2)	2.137(5)	2.179(2)	2.163(4)	2.164(2)	2.174(3)	2.176(4)	2.166(2)	2.172(2)	2.171(2)	2.143(4)	2.144(2)	2.163(2)	2.169(7)
M(3)-O(4)	2.184(3)	2.186(4)	2.199(3)	2.168(6)	2.180(2)	2.198(4)	2.204(2)	2.175(5)	2.206(2)	2.201(4)	2.206(2)	2.211(3)	2.196(5)	2.202(2)	2.200(3)	2.198(2)	2.174(4)	2.181(2)	2.195(2)	2.210(8)
M(3)-O(2)	2.209(3)	2.225(4)	2.225(3)	2.232(5)	2.232(2)	2.238(4)	2.237(2)	2.210(5)	2.245(2)	2.244(4)	2.237(2)	2.246(3)	2.232(5)	2.232(2)	2.218(3)	2.242(2)	2.217(4)	2.214(2)	2.227(2)	2.232(8)
<M(3)-O>	2.155	2.156	2.162	2.145	2.148	2.164	2.173	2.140	2.178	2.170	2.171	2.179	2.171	2.169	2.166	2.173	2.152	2.149	2.162	2.175
$M(4)O_4(OH)_2$ octahedron																				
M(4)-O(4)	2.088(3)	2.080(4)	2.092(3)	2.077(5)	2.083(2)	2.093(3)	2.087(2)	2.074(5)	2.112(2)	2.081(4)	2.095(2)	2.118(3)	2.086(5)	2.089(2)	2.094(3)	2.085(2)	2.088(5)	2.085(2)	2.091(2)	2.097(7)
M(4)-O(4)	2.088(3)	2.080(4)	2.092(3)	2.077(5)	2.083(2)	2.093(3)	2.087(2)	2.074(5)	2.112(2)	2.081(4)	2.095(2)	2.118(3)	2.086(5)	2.089(2)	2.094(3)	2.085(2)	2.088(5)	2.085(2)	2.091(2)	2.097(7)
M(4)-O(1)	2.151(2)	2.142(3)	2.146(3)	2.148(5)	2.137(2)	2.146(4)	2.135(2)	2.145(5)	2.163(2)	2.132(4)	2.149(2)	2.165(3)	2.146(4)	2.141(2)	2.155(2)	2.145(2)	2.158(4)	2.154(2)	2.154(2)	2.149(8)
M(4)-O(1)	2.151(2)	2.142(3)	2.146(3)	2.148(5)	2.137(2)	2.146(4)	2.135(2)	2.145(5)	2.163(2)	2.132(4)	2.149(2)	2.165(3)	2.146(4)	2.141(2)	2.155(2)	2.145(2)	2.158(4)	2.154(2)	2.154(2)	2.149(8)
M(4)-O(3)	2.171(3)	2.165(3)	2.171(3)	2.157(5)	2.159(2)	2.170(4)	2.156(2)	2.163(5)	2.183(2)	2.163(4)	2.184(2)	2.182(3)	2.169(4)	2.170(2)	2.182(2)	2.171(2)	2.170(4)	2.171(2)	2.181(2)	2.181(7)
M(4)-O(3)	2.171(3)	2.165(3)	2.171(3)	2.157(5)	2.159(2)	2.170(4)	2.156(2)	2.163(5)	2.183(2)	2.163(4)	2.184(2)	2.182(3)	2.169(4)	2.170(2)	2.182(2)	2.171(2)	2.170(4)	2.171(2)	2.181(2)	2.181(7)
<M(4)-O>	2.137	2.129	2.136	2.127	2.126	2.136	2.126	2.127	2.153	2.125	2.143	2.155	2.134	2.133	2.144	2.134	2.139	2.137	2.142	2.142
$D \phi_6$ octahedron																				
D-O(2)	1.877(3)	1.835(4)	1.811(3)	1.808(5)	1.797(2)	1.823(3)	1.807(3)	1.844(5)	1.808(2)	1.863(4)	1.887(2)	1.809(3)	1.866(4)	1.876(2)	1.885(3)	1.794(2)	1.894(5)	1.866(2)	1.854(3)	1.929(8)
D-O(12)	1.979(3)	1.958(4)	1.950(3)	1.956(5)	1.957(2)	1.957(3)	1.959(3)	1.936(6)	1.962(2)	1.950(4)	1.968(2)	1.958(3)	1.960(5)	1.956(2)	1.967(3)	1.956(2)	1.984(6)	1.970(3)	1.960(2)	1.998(9)
D-O(11)	1.986(3)	1.962(4)	1.956(3)	1.965(5)	1.958(2)	1.967(3)	1.960(3)	1.945(6)	1.965(2)	1.950(5)	1.974(3)	1.964(3)	1.966(5)	1.967(3)	1.978(3)	1.959(2)	1.998(5)	1.983(3)	1.967(2)	2.001(9)
D-O(9)	1.981(3)	1.956(4)	1.953(3)	1.947(6)	1.958(2)	1.951(3)	1.956(2)	1.945(5)	1.961(2)	1.949(4)	1.965(2)	1.956(3)	1.965(5)	1.957(2)	1.970(3)	1.956(2)	1.990(5)	1.970(2)	1.964(2)	1.987(8)
D-O(15)	1.989(3)	1.966(4)	1.950(3)	1.957(5)	1.962(2)	1.969(3)	1.959(3)	1.950(5)	1.968(2)	1.963(4)	1.973(2)	1.963(3)	1.966(5)	1.964(2)	1.973(3)	1.966(2)	1.996(5)	1.980(2)	1.969(2)	1.994(8)
D-φ(16)	2.104(0)	2.086(1)	2.095(1)	2.094(1)	2.097(0)	2.068(1)	2.084(1)	2.090(1)	2.081(0)	2.037(1)	2.014(0)	2.082(1)	2.034(1)	2.033(0)	2.047(1)	2.086(1)	2.095(1)	2.096(0)	2.056(0)	1.981(1)
<D-φ>	1.986	1.961	1.953	1.955	1.955	1.956	1.954	1.952	1.958	1.952	1.964	1.955	1.960	1.959	1.970	1.953	1.993	1.978	1.962	1.982

TABLE 4. CONTINUED

SAMPLE	LAB3	NOR1	NOR17	RUS4	RUS8	RUS9	RUS12	US5	MSH2	MSH3	MSH8	MSH9	MSH15	MSH15A	MSH19A	MSH20	MSH33A	MSH34	MSH38A	MSH42
T(1) tetrahedron																				
T(1)-O(15)	1.588(3)	1.601(4)	1.605(3)	1.610(6)	1.604(2)	1.602(3)	1.612(3)	1.590(6)	1.611(2)	1.601(5)	1.604(2)	1.611(3)	1.603(6)	1.602(2)	1.603(3)	1.603(2)	1.597(5)	1.595(2)	1.600(2)	1.595(9)
T(1)-O(11)	1.595(3)	1.602(4)	1.601(3)	1.596(5)	1.601(2)	1.603(3)	1.611(3)	1.598(6)	1.610(2)	1.605(5)	1.606(3)	1.612(3)	1.603(5)	1.603(3)	1.603(3)	1.607(2)	1.592(6)	1.594(3)	1.605(2)	1.585(9)
T(1)-O(1)	1.630(3)	1.624(4)	1.623(3)	1.612(5)	1.626(2)	1.630(3)	1.622(3)	1.626(5)	1.626(2)	1.624(5)	1.627(2)	1.625(3)	1.628(5)	1.622(2)	1.627(3)	1.621(2)	1.626(4)	1.625(2)	1.625(2)	1.628(8)
T(1)-O(13)	1.639(3)	1.636(4)	1.644(3)	1.648(5)	1.632(2)	1.648(3)	1.649(3)	1.632(5)	1.645(2)	1.644(5)	1.636(2)	1.640(3)	1.646(5)	1.638(2)	1.641(3)	1.641(2)	1.632(5)	1.628(2)	1.641(2)	1.631(9)
<T(1)-O>	1.613(3)	1.616	1.618	1.617	1.616	1.621	1.624	1.612	1.623	1.619	1.618	1.622	1.620	1.616	1.619	1.618	1.612	1.611	1.618	1.610
T(2) tetrahedron																				
T(2)-O(13)	1.605(3)	1.617(4)	1.613(3)	1.607(5)	1.616(2)	1.614(3)	1.613(2)	1.605(5)	1.618(2)	1.617(5)	1.617(2)	1.619(3)	1.609(5)	1.615(2)	1.613(3)	1.617(2)	1.614(5)	1.618(3)	1.613(2)	1.614(9)
T(2)-O(3)	1.617(3)	1.613(4)	1.609(3)	1.627(6)	1.616(2)	1.623(3)	1.614(3)	1.609(5)	1.615(2)	1.607(5)	1.618(2)	1.620(3)	1.612(5)	1.616(2)	1.621(3)	1.612(2)	1.626(5)	1.620(2)	1.614(2)	1.620(7)
T(2)-O(8)	1.633(3)	1.642(4)	1.635(3)	1.634(5)	1.633(2)	1.639(4)	1.642(3)	1.638(5)	1.641(2)	1.634(4)	1.638(2)	1.637(3)	1.630(5)	1.644(2)	1.645(3)	1.642(2)	1.628(5)	1.636(2)	1.642(2)	1.638(8)
T(2)-O(10)	1.635(3)	1.637(4)	1.637(3)	1.633(5)	1.635(2)	1.639(4)	1.642(3)	1.635(5)	1.642(2)	1.642(4)	1.635(3)	1.638(3)	1.643(5)	1.636(2)	1.642(3)	1.637(2)	1.637(5)	1.636(2)	1.643(2)	1.645(8)
<T(2)-O>	1.622	1.627	1.624	1.625	1.625	1.629	1.628	1.622	1.629	1.625	1.627	1.629	1.624	1.628	1.630	1.627	1.626	1.628	1.628	1.632
T(3) tetrahedron																				
T(3)-O(14)	1.613(3)	1.620(4)	1.605(3)	1.616(5)	1.614(2)	1.613(3)	1.611(3)	1.598(5)	1.615(2)	1.608(5)	1.621(3)	1.618(3)	1.615(5)	1.619(2)	1.614(3)	1.617(2)	1.618(5)	1.619(2)	1.616(2)	1.630(9)
T(3)-O(6)	1.628(3)	1.624(4)	1.612(3)	1.620(5)	1.628(2)	1.633(3)	1.614(3)	1.603(5)	1.625(2)	1.615(5)	1.631(2)	1.622(3)	1.611(5)	1.618(2)	1.624(3)	1.617(2)	1.644(5)	1.631(2)	1.621(2)	1.629(7)
T(3)-O(10)	1.642(3)	1.639(4)	1.637(3)	1.640(5)	1.642(2)	1.652(4)	1.639(3)	1.629(5)	1.642(2)	1.647(4)	1.652(2)	1.648(3)	1.647(5)	1.648(2)	1.645(3)	1.646(2)	1.643(5)	1.645(2)	1.642(2)	1.630(9)
T(3)-O(8)	1.643(3)	1.639(4)	1.640(3)	1.644(6)	1.641(2)	1.651(3)	1.642(2)	1.633(5)	1.644(2)	1.643(4)	1.650(2)	1.653(3)	1.650(5)	1.643(2)	1.640(3)	1.643(2)	1.653(5)	1.645(2)	1.643(2)	1.645(8)
<T(3)-O>	1.6315(3)	1.631	1.624	1.630	1.631	1.637	1.627	1.616	1.632	1.628	1.639	1.635	1.631	1.632	1.631	1.631	1.640	1.635	1.631	1.634
T(4) tetrahedron																				
T(4)-O(9)	1.594(3)	1.598(4)	1.598(3)	1.604(6)	1.601(2)	1.608(3)	1.610(3)	1.585(5)	1.607(2)	1.607(4)	1.606(3)	1.613(3)	1.598(5)	1.606(3)	1.607(3)	1.608(2)	1.595(5)	1.601(3)	1.601(2)	1.591(9)
T(4)-O(12)	1.595(3)	1.601(4)	1.603(3)	1.606(5)	1.601(2)	1.610(3)	1.613(3)	1.597(6)	1.608(2)	1.614(5)	1.606(2)	1.615(3)	1.607(5)	1.604(3)	1.604(3)	1.609(2)	1.595(5)	1.602(3)	1.601(2)	1.591(9)
T(4)-O(7)	1.634(3)	1.625(4)	1.628(3)	1.628(6)	1.628(2)	1.634(3)	1.626(3)	1.623(5)	1.627(2)	1.619(5)	1.625(2)	1.629(3)	1.625(5)	1.626(2)	1.628(3)	1.626(2)	1.625(3)	1.630(2)	1.632(2)	1.613(8)
T(4)-O(14)	1.632(3)	1.629(4)	1.643(3)	1.632(6)	1.632(2)	1.632(3)	1.640(3)	1.641(6)	1.642(2)	1.640(4)	1.629(2)	1.637(3)	1.639(5)	1.633(2)	1.634(3)	1.637(2)	1.624(5)	1.624(3)	1.635(2)	1.607(9)
<T(4)-O>	1.614(3)	1.613	1.618	1.618	1.616	1.621	1.622	1.612	1.621	1.620	1.617	1.624	1.617	1.617	1.618	1.620	1.610	1.614	1.617	1.601
B-O(12)x2	2.624(4)	2.607(5)	2.620(4)	2.589(7)	2.592(3)	2.596(4)	2.599(3)	2.618(7)	2.613(3)	2.628(6)	2.632(3)	2.620(3)	2.645(7)	2.627(3)	2.645(4)	2.610(3)	2.626(7)	2.613(4)	2.612(3)	2.642(15)
B-O(9)x2	2.627(4)	2.612(5)	2.602(4)	2.592(7)	2.592(3)	2.606(4)	2.596(3)	2.626(7)	2.593(3)	2.629(6)	2.614(3)	2.600(4)	2.627(6)	2.626(3)	2.605(4)	2.585(3)	2.617(7)	2.615(3)	2.595(3)	2.641(13)
B-O(11)x2	2.648(4)	2.630(5)	2.634(4)	2.609(7)	2.613(3)	2.600(4)	2.604(3)	2.642(8)	2.614(3)	2.640(6)	2.640(3)	2.611(3)	2.636(6)	2.651(3)	2.667(4)	2.614(3)	2.638(7)	2.639(4)	2.637(3)	2.662(13)
B-O(15)x2	2.618(4)	2.612(5)	2.609(4)	2.589(7)	2.586(3)	2.590(4)	2.610(3)	2.626(8)	2.614(3)	2.634(6)	2.622(3)	2.615(3)	2.635(6)	2.630(3)	2.604(4)	2.601(3)	2.623(7)	2.618(4)	2.601(3)	2.665(14)
B-O(16)x2	2.702(0)	2.693(0)	2.689(0)	2.689(0)	2.688(0)	2.701(0)	2.696(0)	2.681(0)	2.699(0)	2.694(1)	2.710(0)	2.699(0)	2.702(0)	2.702(0)	2.710(0)	2.694(0)	2.709(0)	2.700(0)	2.701(0)	2.715(0)
<B-φ>	2.644	2.631	2.631	2.614	2.614	2.619	2.621	2.639	2.627	2.645	2.644	2.629	2.649	2.647	2.646	2.621	2.643	2.637	2.629	2.665
<K(1a)-φ>	3.288	3.278	3.179	3.268	3.258	3.135	3.265	3.225	3.270	3.272	3.275	3.229	3.272	3.277	3.279	3.260	3.291	3.281	3.268	3.121

TABLE 5. MISCELLANEOUS PARAMETERS FOR POLYHEDRA IN ASTROPHYLLITE-GROUP MINERALS

Sample	LAB 3	NOR 1	NOR 17	RUS 4	RUS 8	RUS 9	RUS 12	US 5	MSH 2	MSH 3
Distortions (quadratic elongation, Δ)										
$\Delta M(1)$	1.854	1.150	0.600	1.116	0.895	0.937	0.732	1.038	0.528	0.737
$\Delta M(2)$	5.431	6.504	6.489	7.946	7.168	6.057	5.657	8.171	6.204	6.136
$\Delta M(3)$	2.236	3.193	3.086	4.245	4.265	3.634	2.897	3.497	3.016	3.581
$\Delta M(4)$	2.740	2.843	2.381	2.829	2.255	2.268	1.845	3.262	1.928	2.530
ΔD	10.939	13.685	17.642	17.931	19.713	13.110	16.846	13.593	16.442	6.685
$\Delta T(1)$	1.839	0.847	1.106	1.411	0.694	1.423	0.893	1.227	0.765	1.116
$\Delta T(2)$	0.573	0.586	0.602	0.447	0.309	0.434	0.767	0.839	0.594	0.718
$\Delta T(3)$	0.561	0.279	0.881	0.557	0.487	0.945	0.749	0.910	0.546	1.089
$\Delta T(4)$	1.425	0.738	1.289	0.607	0.813	0.552	0.536	1.844	0.801	0.577
Octahedron flattening (Ψ, °)										
$\Psi_{M(1)}$	59.392	59.311	58.976	59.488	59.430	59.136	58.919	59.392	58.712	58.865
$\Psi_{M(2)}$	59.400	59.189	58.866	59.321	59.277	58.957	58.686	59.518	58.729	58.463
$\Psi_{M(3)}$	59.296	59.011	58.673	59.174	59.040	58.889	58.578	59.200	58.465	58.558
$\Psi_{M(4)}$	59.292	59.102	58.882	59.445	59.243	58.993	58.430	59.514	58.677	58.472
$\Psi_{average}$	59.345	59.153	58.849	59.357	59.248	58.993	58.653	59.406	58.646	58.590
Octahedron angle variance (σ)										
$\sigma_{M(1)}$	61.09	60.06	57.81	61.97	62.60	56.47	57.43	60.46	52.50	56.54
$\sigma_{M(2)}$	52.77	49.59	45.53	51.47	50.79	45.48	43.37	54.52	43.52	38.53
$\sigma_{M(3)}$	49.91	44.56	40.81	47.49	44.88	42.34	39.30	47.47	37.81	38.27
$\sigma_{M(4)}$	48.56	44.85	42.02	51.61	47.80	43.03	33.04	53.75	38.51	33.10
σD	50.428	50.126	52.818	61.601	63.327	53.454	57.420	46.866	54.718	30.996
Tetrahedron tilting [°, with respect to (001)]										
$TT(1)$	7.19	6.85	6.75	6.62	6.94	6.64	6.49	6.91	7.27	6.00
$TT(2)$	2.12	2.00	2.32	2.17	1.95	1.82	2.60	1.57	2.15	2.65
$TT(3)$	0.93	0.78	1.17	0.81	0.78	0.80	1.02	0.39	0.83	1.18
$TT(4)$	7.34	7.14	7.04	7.24	7.25	6.92	7.35	7.23	7.53	6.82
Tetrahedron rotation (α, °)										
$\alpha_{T(ave)}$	1.07	1.06	1.11	0.86	1.03	1.37	1.42	0.93	1.56	1.26
Tetrahedron thickening angle (τ, °)										
$\tau_{T(1)}$	111.45	111.58	111.16	111.76	111.63	111.35	111.44	111.07	111.28	111.39
$\tau_{T(2)}$	110.82	110.95	111.06	111.03	110.91	110.99	111.09	110.81	110.76	111.34
$\tau_{T(3)}$	111.09	111.34	111.32	111.35	111.27	111.31	111.33	111.35	111.18	111.65
$\tau_{T(4)}$	111.57	111.60	111.37	111.72	111.79	111.46	111.59	111.31	111.50	111.53

Sample	MSH 8	MSH 9	MSH 15	MSH 15A	MSH 19A	MSH 20	MSH 33A	MSH 34	MSH 38A	MSH 42
Distortions (quadratic elongation, Δ)										
$\Delta M(1)$	0.956	0.488	0.650	0.782	0.526	0.594	2.851	1.944	0.910	1.041
$\Delta M(2)$	6.275	5.606	6.512	5.925	6.343	6.144	5.106	6.467	6.356	6.059
$\Delta M(3)$	3.057	3.043	2.729	2.892	2.516	3.026	2.485	2.930	3.126	2.470
$\Delta M(4)$	2.919	1.578	2.689	2.467	2.948	2.849	2.859	3.029	3.099	2.611
ΔD	3.729	16.390	6.254	5.415	5.684	18.877	8.531	11.347	8.914	1.526
$\Delta T(1)$	0.711	0.526	1.256	0.847	1.011	0.844	1.175	0.992	1.023	1.558
$\Delta T(2)$	0.346	0.306	0.726	0.597	0.695	0.614	0.254	0.275	0.794	0.961
$\Delta T(3)$	0.630	0.889	1.196	0.696	0.578	0.715	0.630	0.441	0.554	0.166
$\Delta T(4)$	0.430	0.375	0.964	0.599	0.642	0.562	0.840	0.642	1.014	0.370
Octahedron flattening (Ψ, °)										
$\Psi_{M(1)}$	59.058	58.690	58.902	59.015	59.140	58.797	59.438	59.567	59.111	58.913
$\Psi_{M(2)}$	58.937	58.685	58.659	58.831	59.123	58.750	59.358	59.678	59.070	58.788
$\Psi_{M(3)}$	58.779	58.396	58.736	58.760	58.982	58.599	59.523	59.462	58.892	58.726
$\Psi_{M(4)}$	58.891	58.614	58.799	58.799	59.076	58.566	59.510	59.520	59.077	58.786
$\Psi_{average}$	58.916	58.596	58.774	58.851	59.080	58.678	59.457	59.542	59.037	58.803
Octahedron angle variance (σ)										
$\sigma_{M(1)}$	56.35	53.19	55.88	57.90	56.82	54.77	60.09	62.31	56.73	53.24
$\sigma_{M(2)}$	45.70	43.32	41.69	44.53	48.46	43.65	51.24	57.14	47.36	41.00
$\sigma_{M(3)}$	41.34	36.73	41.72	41.57	44.93	39.02	53.50	50.73	43.34	40.41
$\sigma_{M(4)}$	40.56	37.97	39.21	39.30	44.49	35.91	52.49	53.49	44.70	38.70
σD	27.831	54.264	30.505	29.557	35.630	58.574	49.224	51.897	43.279	15.513
Tetrahedron tilting [°, with respect to (001)]										
$TT(1)$	6.64	7.40	6.52	6.47	6.95	6.79	7.44	7.14	6.81	6.31
$TT(2)$	1.92	1.81	2.24	2.14	1.88	2.10	1.83	1.72	1.85	2.28
$TT(3)$	0.81	0.80	1.20	1.06	0.88	0.86	0.82	0.58	0.80	0.87
$TT(4)$	6.74	7.33	6.65	6.69	6.90	7.25	7.25	7.33	6.90	6.87
Tetrahedron rotation (α, °)										
$\alpha_{T(ave)}$	1.39	1.81	1.27	1.25	1.33	1.58	1.18	0.93	1.21	1.49
Tetrahedron thickening angle (τ, °)										
$\tau_{T(1)}$	111.38	111.17	111.23	111.31	111.19	111.34	111.73	111.59	111.42	111.44
$\tau_{T(2)}$	110.87	110.80	111.10	110.99	111.13	110.96	110.76	110.87	110.89	110.76
$\tau_{T(3)}$	111.22	111.25	111.56	111.41	111.35	111.37	110.96	111.15	111.40	111.09
$\tau_{T(4)}$	111.54	111.35	111.48	111.55	111.49	111.59	111.56	111.75	111.62	111.79

SREF indicated departures from unity and the presence of a heavier X-ray scatterer, either Nb or Zr, in accordance with electron-microprobe data, was refined at D, with the total site-occupancy constrained to be unity. There is no evidence from Mössbauer spectroscopy for Fe^{3+} at D.

As EMPA results indicate only minor Al (maximum 0.36 *apfu*) to be present, and Mössbauer spectra did not indicate $^{[4]}Fe^{3+}$, all four T sites were modeled assuming only Si to be present. Site-scattering refinements of the four T sites in all samples did not indicate significant departures from unity.

Bond-valence sums (BVS) indicate the presence of 13 general positions occupied by divalent anions, two general positions for monovalent anions in the O sheet [O(4) and O(5)], and a mixed-valence anion site, $\phi(16)$. Bond-valence sums for all anions [except O(4), O(5) and $\phi(16)$] range from 1.842 to 2.140 valence units (*vu*),

confirming their identity as O^{2-}. The O(2) anion, bonded to $M(1)$, $M(2)$, $M(3)$ and D, has a consistently low BVS (1.842 to 1.973 *vu*, average: 1.903 *vu*) owing to the presence of Na in $M(1)$ and high field-strength elements (HFSE) at D, which contribute less than the required 1 *vu* (Ti^{4+}: 4/6 *vu*, Nb^{5+}: 5/6 *vu*); all other divalent anions in the O sheet are coordinated by three M cations ($3 \times 2/6 = 1$ *vu*) and one T cation ($1 \times 4/4 = 1.00$ *vu*). Consequently, to compensate for this bond-valence deficiency, the $M(1)$–O(2) bond is shortened by, on average, 0.03 Å compared to the average <$M(1)$–O>. Bond-valence sums to O(4) and O(5) range from 0.985 to 1.177 *vu* (average: 1.089 *vu*), indicating the presence of a monovalent anion. Piilonen *et al.* (2003) discussed the pattern of order of OH and F at the O(4), O(5) and $\phi(16)$ sites, and concluded, on the basis of results from EMPA, Mössbauer spectroscopy and thermodynamic calculations, that the sites present in the O sheet [O(4) and O(5)]

TABLE 6. SELECTED BOND-VALENCE SUMS AND SITE OCCUPANCIES IN ASTROPHYLLITE-GROUP MINERALS

Site	BVS	SOF	BVS	SOF	BVS	SOF
		LAB3		US5		MSH19A
B	1.114	$Na_{0.758}Ca_{0.242}$	0.950	$Na_{0.958}$	1.068	$Na_{0.834}Ca_{0.166}$
$M(1)$	1.826	$Fe_{0.876}Na_{0.124}$	1.915	$Fe_{0.891}Na_{0.109}$	2.040	$Mn_{0.912}Na_{0.088}$
$M(2)$	1.877	$Fe_{0.956}$	1.958	$Fe_{1.00}$	2.101	$Mn_{0.986}$
$M(3)$	1.932	$Fe_{0.944}$	2.012	$Fe_{1.00}$	2.118	$Mn_{0.974}$
$M(4)$	2.004	$Fe_{0.872}Mg_{0.128}$	2.084	$Fe_{1.00}$	1.962	$Fe_{0.854}Mg_{0.146}$
D	4.439	$Ti_{0.575}Zr_{0.425}$	4.461	$Ti_{0.769}Nb_{0.231}$	4.063	$Ti_{0.646}Nb_{0.354}$
OH(4)	1.029	$O_{1.00}$	1.068	$O_{1.00}$	1.090	$O_{1.00}$
OH(5)	1.012	$O_{1.00}$	1.077	$O_{1.00}$	1.141	$O_{1.00}$
$\phi(16)$	1.272	$F_{1.00}$	1.202	$F_{1.00}$	1.340	$F_{1.00}$
		NOR1		MSH2		MSH20
B	1.222	$Na_{0.642}Ca_{0.358}$	1.248	$Na_{0.618}Ca_{0.382}$	1.268	$Na_{0.590}Ca_{0.410}$
$M(1)$	2.054	$Mn_{0.887}Na_{0.113}$	1.984	$Mn_{0.891}Na_{0.109}$	1.987	$Mn_{0.873}Na_{0.127}$
$M(2)$	1.842	$Fe_{0.955}$	2.049	$Mn_{0.994}$	2.090	$Mn_{0.999}$
$M(3)$	1.802	$Fe_{0.936}$	2.081	$Mn_{0.985}$	2.128	$Mn_{0.992}$
$M(4)$	2.004	$Fe_{0.850}Mg_{0.150}$	2.236	$Mn_{0.954}Mg_{0.046}$	1.872	$Zn_{0.696}Mg_{0.304}$
D	4.290	$Ti_{0.822}Nb_{0.178}$	4.226	$Ti_{0.910}Nb_{0.090}$	4.181	$Ti_{0.646}Nb_{0.354}$
OH(4)	0.985	$O_{1.00}$	1.114	$O_{1.00}$	1.070	$O_{1.00}$
OH(5)	1.074	$O_{1.00}$	1.108	$O_{1.00}$	1.123	$O_{1.00}$
$\phi(16)$	1.166	$F_{1.00}$	1.162	$F_{1.00}$	1.122	$F_{1.00}$
		NOR17		MSH3		MSH33A
B	1.078	$Na_{0.882}Ca_{0.118}$	0.934	$Na_{0.964}$	1.140	$Na_{0.72}Ca_{0.28}$
$M(1)$	2.024	$Mn_{0.898}Na_{0.102}$	1.932	$Mn_{0.741}Na_{0.109}$	1.065	$Mn_{1.001}$
$M(2)$	2.114	$Mn_{0.985}$	2.122	$Mn_{1.011}$	1.775	$Fe_{0.960}$
$M(3)$	2.209	$Mn_{1.000}$	2.155	$Mn_{0.996}$	1.856	$Fe_{0.954}$
$M(4)$	2.362	$Mn_{1.000}$	1.918	$Zn_{0.766}Mg_{0.234}$	1.994	$Fe_{0.876}Mg_{0.124}$
D	4.308	$Ti_{0.900}Nb_{0.100}$	4.621	$Ti_{0.624}Nb_{0.376}$	4.515	$Ti_{0.462}Zr_{0.538}$
OH(4)	1.177	$O_{1.00}$	1.081	$O_{1.00}$	1.008	$O_{1.00}$
OH(5)	1.140	$O_{1.00}$	1.117	$O_{1.00}$	1.004	$O_{1.00}$
$\phi(16)$	1.216	$F_{1.00}$	1.522	$F_{1.00}$	1.328	$F_{1.00}$
		RUS4		MSH8		MSH34A
B	1.330	$Na_{0.56}Ca_{0.44}$	1.036	$Na_{0.898}Ca_{0.102}$	1.140	$Na_{0.748}Ca_{0.252}$
$M(1)$	2.073	$Mn_{0.91}Na_{0.09}$	1.972	$Mn_{0.863}Na_{0.137}$	2.114	$Mn_{0.997}$
$M(2)$	1.863	$Fe_{0.958}$	2.074	$Mn_{0.985}$	1.851	$Fe_{0.970}$
$M(3)$	1.958	$Fe_{0.86}Mg_{0.14}$	2.098	$Mn_{0.974}$	1.889	$Fe_{0.962}$
$M(4)$	2.034	$Fe_{0.784}Mg_{0.216}$	2.242	$Mn_{0.964}$	2.012	$Fe_{0.922}Mg_{0.078}$
D	4.200	$Ti_{0.965}Nb_{0.035}$	4.528	$Ti_{0.553}Nb_{0.447}$	4.472	$Ti_{0.462}Zr_{0.538}$
OH(4)	1.047	$O_{1.00}$	1.126	$O_{1.00}$	1.018	$O_{1.00}$
OH(5)	1.065	$O_{1.00}$	1.126	$O_{1.00}$	1.059	$O_{1.00}$
$\phi(16)$	1.114	$F_{1.00}$	1.480	$F_{1.00}$	1.256	$F_{1.00}$
		RUS8		MSH15		MSH38A
B	1.320	$Na_{0.582}Ca_{0.418}$	1.028	$Na_{0.88}Ca_{0.12}$	1.152	$Na_{0.772}Ca_{0.228}$
$M(1)$	2.067	$Mn_{0.900}Na_{0.100}$	1.956	$Mn_{0.863}Na_{0.137}$	2.025	$Mn_{0.897}Na_{0.103}$
$M(2)$	1.809	$Fe_{0.946}$	2.133	$Mn_{0.985}$	2.139	$Mn_{0.995}$
$M(3)$	2.031	$Fe_{0.847}Mg_{0.153}$	2.095	$Mn_{0.985}$	2.174	$Mn_{0.978}$
$M(4)$	2.034	$Fe_{0.770}Mg_{0.230}$	2.288	$Mn_{0.964}$	2.278	$Mn_{0.978}$
D	4.234	$Ti_{0.958}Zr_{0.042}$	4.511	$Ti_{0.553}Nb_{0.447}$	4.291	$Ti_{0.787}Nb_{0.213}$
OH(4)	1.059	$O_{1.00}$	1.143	$O_{1.00}$	1.165	$O_{1.00}$
OH(5)	1.029	$O_{1.00}$	1.128	$O_{1.00}$	1.147	$O_{1.00}$
$\phi(16)$	1.124	$F_{1.00}$	1.394	$F_{1.00}$	1.262	$F_{1.00}$

BVS: bond-valence sum, expressed in valence units; SOF: refined site-occupancy factor. Bond-valence sums for RUS9 and RUS12 can be found in Piilonen *et al.* (2001), and for MSH42, in Piilonen *et al.* (2000). The bond-valence sums were calculated using parameters taken from Brese & O'Keeffe (1991).

are occupied solely by OH, whereas $\phi(16)$ hosts both F and O. Bond-valence sums to $\phi(16)$ are variable, ranging from 1.105 to 1.86 *vu* (average: 1.293 *vu*), consistent with the proposed F $\Leftrightarrow$ O substitution at this site. An attempt was made to refine the site occupancy of $\phi(16)$ with both F and O, but results did not prove to be valid owing to low total F contents (<1.00 *apfu*). Bond-valence sums confirm the anionic scheme $O_{26}(OH)_4$ (F,O,$\square$) proposed by Piilonen *et al.* (2003).

THE INTERLAYER SITE

The *A* cations are located in large, [13]-coordinated cavities between adjacent *H*-sheet (Fig. 4) that are occupied predominantly by K and, to a lesser extent, Cs, Rb, Na and $\square$. Large anisotropic-displacement factors along U_{11}, coupled with a large positive residual in the difference-Fourier map (>2.5 e^{-1}) in the majority of the triclinic samples, suggest that this site is positionally disordered within (001). As such, the position was refined as two non-equivalent sites with coordinates taken from the difference-Fourier map. The magnitude of the splitting in the samples analyzed is between 0.360(19) to 0.917(18) Å in (001). A decrease in displacement factors is observed if the site is modeled as positionally disordered, similar to what is observed in amphiboles with high *A*-site occupancies (Hawthorne 1981).

One of the main differences between the structures of monoclinic and triclinic kupletskite, aside from the *HOH* stacking sequence, is the degree of disorder at the *A* site (Piilonen *et al.* 2001). In triclinic kupletskite from the Lovozero massif (Russia), the *A* site shows positional disorder comparable to that observed in other triclinic samples [*A*(1a)–*A*(1b) = 0.917 Å]. However, in kupletskite-*Ma2b2c*, the *A* cation lies on two special positions, both of which have well-constrained anisotropic-displacement factors (U_{eq} = 0.0451 Å).

Bond lengths to *A* range from 2.826(4) to 3.721(3) Å. The *A*(1a) site in disordered triclinic samples is generally [11]-coordinated, with longer average bond-lengths (range: 3.179 to 3.291 Å) than those observed at the [5]- to [7]-coordinated *A*(1b) satellite position (range: 2.353 to 3.082 Å). The overall coordination of the *A* site in both triclinic and monoclinic samples is [13].

The *B* site is located at a special position in [10]-coordinated cages along *a* between $D\phi_6$ pairs ($BO_8\phi_2$, Fig. 5) and is occupied predominantly by Na and, to a lesser extent, Ca (up to 0.40 *apfu*). There is no evidence for other cations or vacancies at *B*. The *B*–ϕ distances range from 2.585(3) to 2.715 Å, with an average of 2.635 Å.

THE (*O*) SHEET OF OCTAHEDRA

There are four crystallographically distinct *O*-sheet octahedra, designated *M*(1) through *M*(4), which occur in a 2:2:2:1 ratio, respectively. The *O* sheet can be di-

vided into three main units: (1) a strip of $M(2)$ octahedra, linked *via* common edges, which form continuous zigzag single chains parallel to [100], (2) a composite chain parallel to [100] comprised of alternating $M(3)$

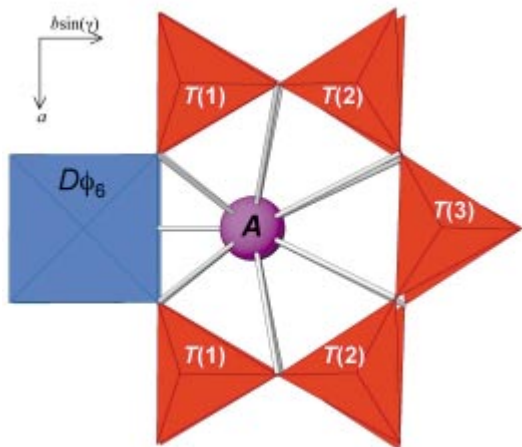FIG. 4.   The configuration of the H-sheet chains around the A site in (001). Upper chain shown. Lower chain (clockwise): $T(4)$, $T(3)$, $T(2)$, $T(3)$ and $T(4)$. Distances range from 2.825(4) to 3.721(3) Å. Splitting of the A site results in displacement of the A cation along $b\sin(\gamma)$ of 0.360(19) to 0.917(18) Å.
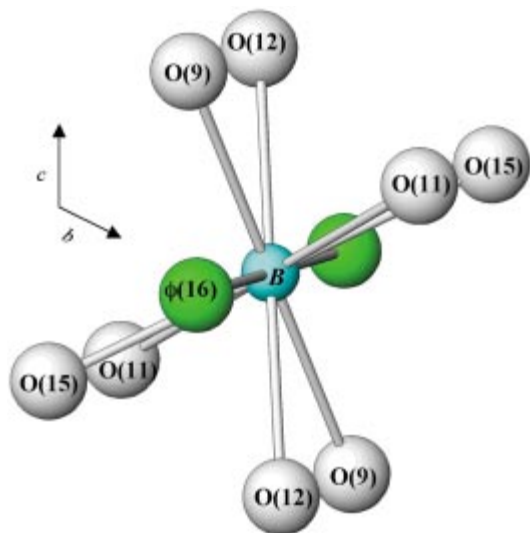
FIG. 5.   The $BO_8\phi_2$ polyhedron. Distances range from 2.585(3) to 2.715 Å.

and $M(4)$ octahedra in a 2:1 ratio, and (3) isolated $M(1)$ octahedra that cross-link the two chains of octahedra (Fig. 6). The combination of chain-like structural elements within the O sheet and open-branched, *zweier*, single [100] chains in the H sheet has a pronounced effect on the morphology of astrophyllite-group minerals: a preferential elongation of crystals in the [100] direction (resulting in the formation of acicular to tabular crystals), and the development of a secondary, moderate parting along {010}. The O sheet is joined to the H sheet *via* apical atoms of oxygen from the H-sheet tetrahedra [O(1), O(3), O(6) and O(7)] and *via* the $D\phi_6$ apical oxygen, O(2) (Fig. 7).

The steric details of the O sheet must be examined in order to characterize the control it exerts on cation ordering and its subsequent impact on the adjacent H-sheets. As a general parameter, the grand mean bond-length, $<<M$–$O>>$, allows for comparison of the relative dimensions of the O sheet among species. The variation in $<<M$–$O>>$ as a function of grand mean ionic radius, $<<\mathrm{r}M>>$, is shown in Figure 8. The high degree of correlation ($R^2 = 0.938$) is described by the linear-regression equation $<<M$–$O>> = 1.752 + 1.183\mathrm{r}M$. The scatter observed in the trend may be due to the slight differences between refined site-occupancies and EMPA data from which $<<\mathrm{r}M>>$ was calculated. Whereas it is important to examine the relation between $<<M$–$O>>$ and $<<\mathrm{r}M>>$ in the O sheet, the ligancy and local environment of each of the four individual octahedra vary from sample to sample. Unfortunately, owing to the presence of multiple cations at all four M sites, coupled with difficulties in refining the SOF of sites containing both Mn and Fe, only poor correlations are observed between the calculated average ionic radii at each M site and $<M$–$O>$ (*i.e.*, $0.341 \leq R^2 \leq 0.710$).

The distortion index, calculated for each individual octahedron, is a direct reflection of the local environment of the cation and therefore sensitive to variations in site chemistry, bond lengths and bond angles. Table 6 lists values for two distortion parameters, Δ, the bond-length distortion, and σ, the octahedron angle variance (OAV), for each octahedron. Calculation of Δ takes into consideration the average cation radius by normalizing the parameter to the average bond-length, and also corrects for the coordination number. Consequently, Δ is a measure of distortions within the polyhedra resulting from stretching or compression of M–O bonds (commonly referred to as rectangular distortions), which violate the ideal trigonal symmetry of the octahedron. Conversely, the OAV takes into consideration only the angular variance within the octahedron. In astrophyllite-group minerals, a discrepancy is noted between the two parameters such that Δ indicates the relative degree of distortion, represented by the sequence $M(2) > M(3,4) > M(1)$, whereas the OAV indicates the sequence $M(1) > M(2) > M(3) > M(4)$, which also corresponds to the order of decreasing size of each of the M octahedra. In the O sheet, the OAV is not an adequate measure of the
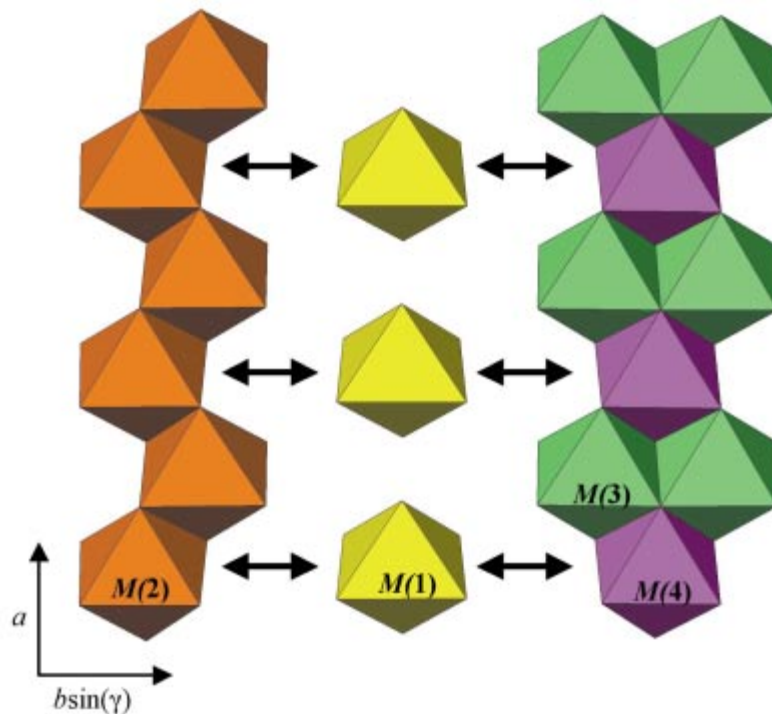
FIG. 6.   The three main units of the *O* sheet. The *M*(2) octahedra form chains parallel to [100]. *M*(3) and *M*(4) alternate along [100] in a 2:1 ratio. *M*(1), the largest and least distorted of the octahedra, links the two composite strips together to form infinite sheets in (001).
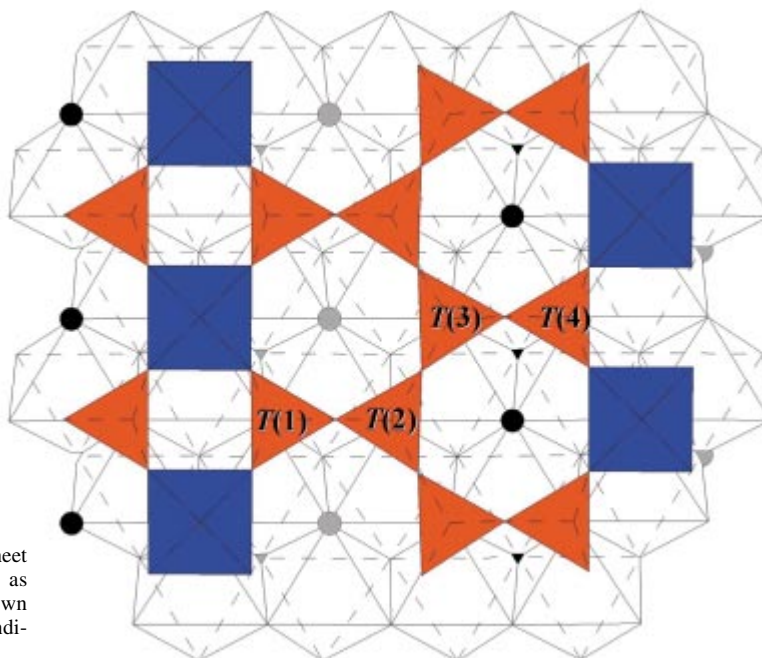
FIG. 7.   The attachment of the *H* sheet to the *O* sheet. *T* sites: orange as indicated, *D*: blue, *M* sites shown outlined. The OH groups are indicated as solid circles.

total distortion of each octahedron, as it does not take into account rectangular distortions (*i.e.*, stretching or compression of bond lengths within the octahedron); the OAV can only be considered as a reflection of trigonal distortions (*i.e.*, compression or extension of the octahedron, resulting in a flattened octahedron whose M–O distances remain equal in length; Robinson *et al.* 1971). In particular, the OAV exhibits a strong, positive correlation with the octahedron flattening angle, Ψ, and the two terms may be used interchangeably. Figure 9 shows the relation between OAV and Ψ for each of the four O-sheet octahedra. The less-than-ideal correlation for the $M(1)$ octahedron will be discussed in further sections. Ideally, in octahedra that have undergone both rectangular and isometric or trigonal distortions, both the Δ and OAV/Ψ distortion parameters should be taken into account in describing the geometry of a given octahedron.

The $M(1)$ site is coordinated by five O^{2-} and one OH(5), and is host to Mn, Fe^{2+} and up to 0.27 *apfu* Na. The resultant octahedron is the largest in the O sheet and occurs as isolated octahedra, which bridge composite chains of $M(2)$ and $M(3,4)$. Figure 10 shows the regular distribution of bond lengths in $M(1)$, which range from 2.137(5) to 2.247(7) Å, with an average of 2.195 Å, close to the ideal for a $^{[6]}Mn^{2+}$–O bond (2.21 Å; Ondik & Smith 1962). This regular distribution of bond lengths is consistent with $M(1)$ being the least distorted of the four octahedra; Δ values range from 0.488 to 2.851.

In an ideal octahedron, the flattening angle, Ψ, measured at the point between the M–O bond and a line perpendicular to the upper and lower trigonal faces through the central cation, is 54.74°. Flattening of the
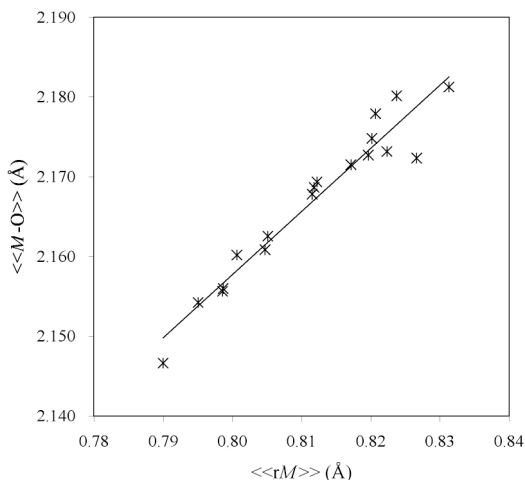
FIG. 8.   Variation in grand mean M–O bond length, $<<M$–$O>>$, with mean ionic radius, $<<rM>>$, for the O sheet. Linear regression, $R^2 = 0.938$.

octahedron in the (001) plane, in order to facilitate lateral fit with the larger H sheets, results in values of Ψ greater than the ideal. Typical values for Ψ in sheet silicates range from 58 to 60° (Bailey 1984). In general, average Ψ angles are negatively correlated with the average ionic radius, rM, or the size of the octahedra (Fig. 11). Although $M(1)$ is the largest of the four O-sheet octahedra, it displays the greatest degree of flattening, with Ψ values ranging from 58.7 to 59.6° (average: 59.1°). This finding is opposite to that predicted, possibly because flattening must occur within the (001) plane to permit bridging with the adjacent chains of $M(2)$ and $M(3,4)$ octahedra (Fig. 6).

The $M(2)$ and M(3) sites, host to Mn, Fe, Mg and Zn, are both coordinated by four O^{2-} and two OH^-, with a *cis* configuration of the OH^- groups [$M(2)$: OH(5) × 2, $M(3)$: OH(4) × 2]. The $M(2)$ site is unique in the structure as it forms continuous, zigzag chains of edge-sharing octahedra parallel to [100]; all other M sites share, at most, one common edge with crystallographically equivalent octahedra. Bond lengths in $M(2)$ range from 2.079(5) to 2.267(2) Å. The $M(2)$ octahedron is elongate across the O(2)–$M(2)$–O(7) linkage, and shortened along M–OH(5) bonds along the shared edges, resulting in a bimodal distribution of bond lengths (Fig. 10). The irregular distribution of bond lengths results in a strong rectangular distortion of $M(2)$; Δ values range from 5.106 to 8.171 (average: 6.319) with flattening angles that are similar to those observed for $M(1)$, ranging from 58.5 to 59.7° (average: 59.0°).

The $M(3)$ octahedron is part of a composite chain parallel to *a*, and consists of alternating $M(3)$ and $M(4)$ octahedra in a 2:1 ratio. Both octahedra are only slightly distorted relative to $M(2)$ [Δ_{ave}: 3.104 and 2.600 for $M(3)$ and $M(4)$, respectively]. Bond lengths to $M(3)$ range from 2.098(5) to 2.246(3) Å, with an average of 2.163 Å. Unlike bond lengths in the $M(2)O_6$ octahedron, $M(3)O_6$ bond lengths are regularly distributed, with only a slight skew toward values close to 2.135 Å (*i.e.*, the ideal Fe^{2+}–O bond length of 2.14 Å: Ondik & Smith 1962). This observation is consistent with the hypothesis that Fe^{2+} preferentially orders at $M(2)$, $M(3)$ and $M(4)$ over $M(1)$.

The $M(4)$ site occupies special position 1*g* in triclinic astrophyllite-group minerals and 4*c* in kupletskite-*Ma*2*b*2*c*. The $M(4)$ octahedron, the smallest in the O sheet (volume range: 12.551 to 13.111 Å^3), is coordinated by four O^{2-} and two OH^-, with a *trans* configuration of the OH groups [2 × OH(4)]. Bond lengths to $M(4)$ range from 2.074(5) to 2.184(2) Å (average: 2.136 Å). A bimodal distribution of bond lengths is observed (Fig. 10), as distances to the two OH(4) anions are short [range: 2.074(5) to 2.118(3) Å] and those to the four O^{2-} are longer [range: 2.132(4) to 2.184(2) Å]. Site-occupancy refinement indicates ordering of small divalent cations (Mg and Zn) extensively at both $M(3)$ and $M(4)$ relative to $M(2)$.
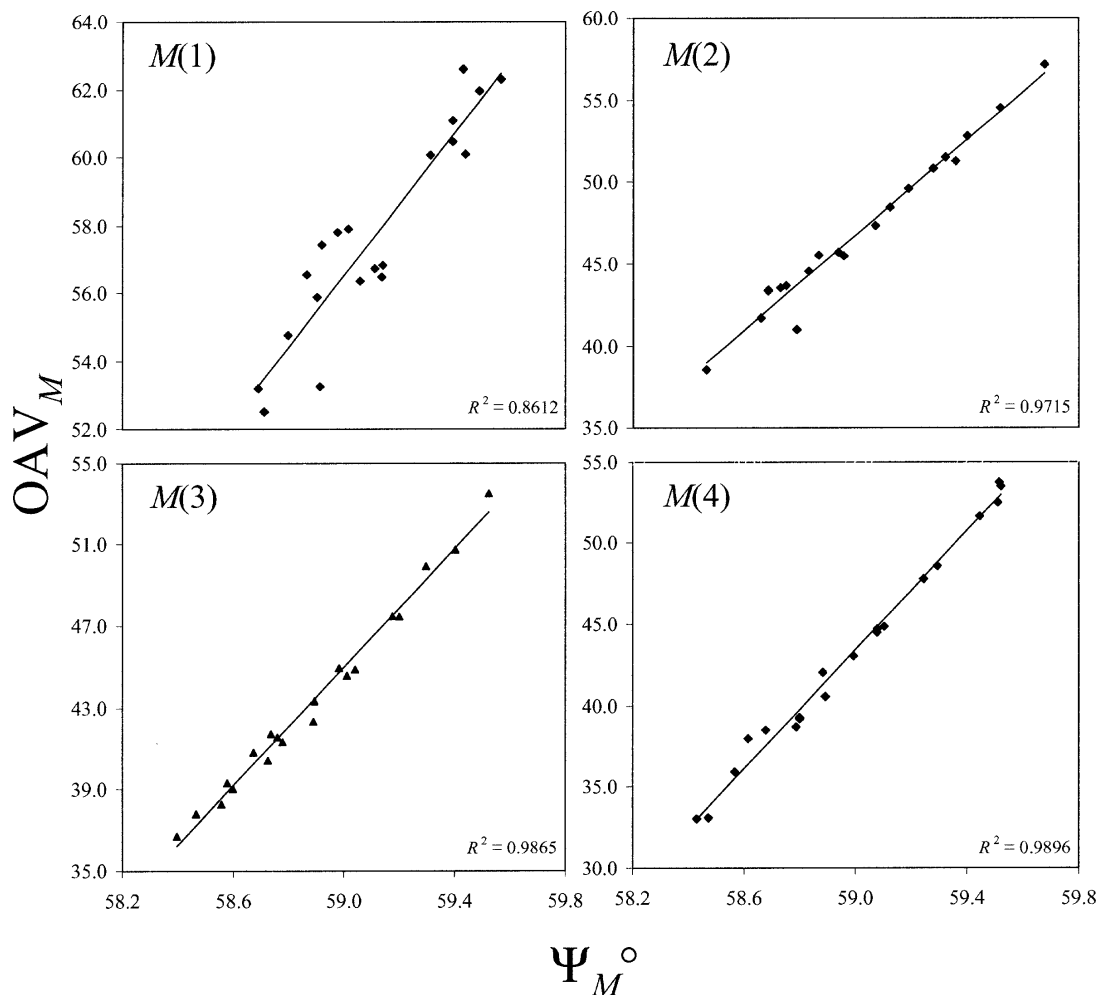
FIG. 9. Degree of flattening of the octahedra (Ψ) *versus* the octahedron angle variance (OAV) for each of the M sites in the O sheet.

THE HETEROGENEOUS (H) SHEET

The $D\phi_6$ octahedron

The D site in triclinic astrophyllite-group minerals and kupletskite-$Ma2b2c$ is coordinated by five O and by $\phi(16)$, a mixed-anion site containing F and O. Apical anions include O(2), which is also bonded to $M(1)$, $M(2)$ and $M(3)$ in the O sheet, and $\phi(16)$. Basal anions include O(9) and O(12), which are bonded to $T(4)$, and O(11) and O(15), which are bonded to $T(1)$. In magnesium astrophyllite, the $\phi(16)$ site is vacant, resulting in a DO_5 tetragonal pyramid (Shi *et al.* 1998). All structures in this study were found to contain octahedrally coordinated D cations, with Ti contents ranging from

0.24 to 1.92 *apfu*, Nb contents from 0.06 to 1.33 *apfu*, and Zr contents from below detection up to 0.72 *apfu* (Table 2). The D site was modeled as hosting Ti and one of either Nb or Zr. As both Nb and Zr are heavier X-ray scatterers than Ti, the difference between unity and the refined Ti content is considered to be equivalent to the sum of Nb + Zr. Bond-valence sums to D range from 4.064 *vu* in Zr- and Nb-free astrophyllite to 4.800 *vu* in niobokupletskite.

A wide range of bond lengths is observed in the $D\phi_6$ octahedron [range: 1.794(2) to 2.104 Å], a combined result of the octahedron being highly distorted and elongate along the pseudo-tetrad axis and the presence of variable proportions of Ti, Nb and Zr. The average D–ϕ bond length, $<D–\phi>$, is a function of the average ionic

radius of the cations at the *D* site, as shown in Figure 12. As the radii of Ti and Nb are similar ($r^{[6]}Ti^{4+}$: 0.61 Å, $r^{[6]}Nb^{5+}$: 0.64 Å, Shannon 1976), variations in the size of the $D\phi_6$ octahedron can only be attributed to the presence of Zr ($r^{[6]}Zr^{4+}$: 0.72 Å, Shannon 1976). Although substitution of Nb for Ti does not affect the overall size of the $D\phi_6$ octahedron significantly, it does have a pronounced control on the bond-length variations, in particular the distribution of apical bond-lengths, as will be discussed in further sections. In other titano-, niobo- or zirconosilicates, such as rosenbuschite, seidozerite and vuonnemite, the extent of isomorphous substitution of both Zr and Nb for Ti is limited and, in the majority

of minerals, there is a high degree of order among species. The presence of (Ti + Nb + Zr) at a single site in minerals of this group gives us the unique opportunity to examine the local geometry and bond-valence requirements imposed on the structure by all three elements.

The average distance to the four equatorial oxygen atoms is 1.966 Å, close to the ideal length of 1.98 Å for a Ti–O bond (Ondik & Smith 1962) and slightly less than observed in other alkali titanosilicates with [6]-coordinated Ti [*e.g.,* seidozerite: Simonov & Belov (1960), lomonosovite: Khalilov (1990), tienshanite: Cooper *et al.* (1998), vuonnemite: Ercit *et al.* (1998)]. Bond lengths to O(9) and O(12) are, on average, slightly shorter than bond lengths to the opposite O(11) and O(15) (average: 1.962 and 1.969 Å, respectively). Angles between equatorial oxygen atoms range from 87.2(3) to 90.6(6)° (average: 88.9°), close to the ideal 90°. Apical bond-lengths display the greatest range in values, from 1.794(2) to 2.104 Å, and have a strong bimodal distribution (Fig. 13), a result of positional displacement of the cation within the octahedron. In general, D–O(2) bonds are the shortest (average: 1.845 Å), ranging from 1.794(2) Å in Nb- and Zr-free kupletskite, to 1.929(8) Å in niobokupletskite. However, D–φ(16) bond lengths are relatively long (average: 2.069 Å), ranging from 1.981(1) Å in MSH42 (niobokupletskite), to 2.104 Å in LAB3 (Zr-bearing astrophyllite, Fig. 14). A bimodal distribution of apical bond-lengths in TiO_6 octahedra is a common feature in other titanosilicates (Table 7). Megaw (1968a, b) suggested that off-center displacement of small, highly
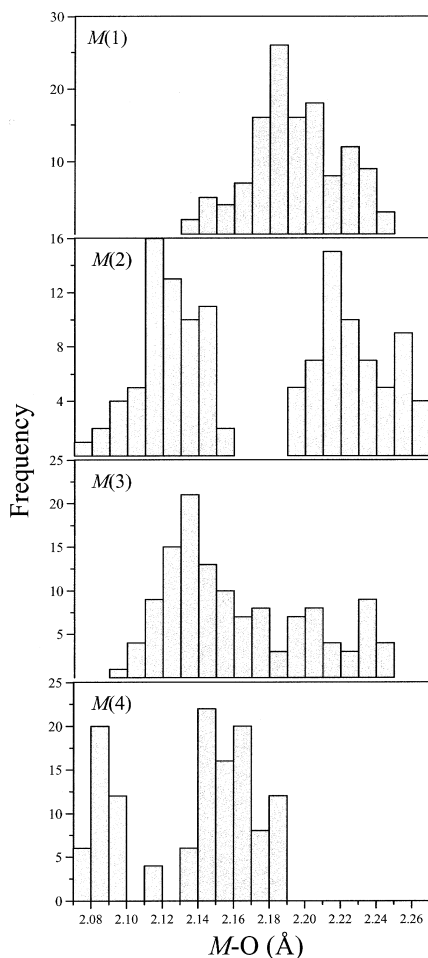
FIG. 10. Frequency histograms of *M*–O bond distances in the *O* sheet of astrophyllite-group minerals. *M*(1): 2.137(5) to 2.247(7) Å, *M*(2): 2.079(5) to 2.267(2) Å, *M*(3): 2.098(5) to 2.246(3) Å, and *M*(4): 2.074(5) to 2.184(2) Å.
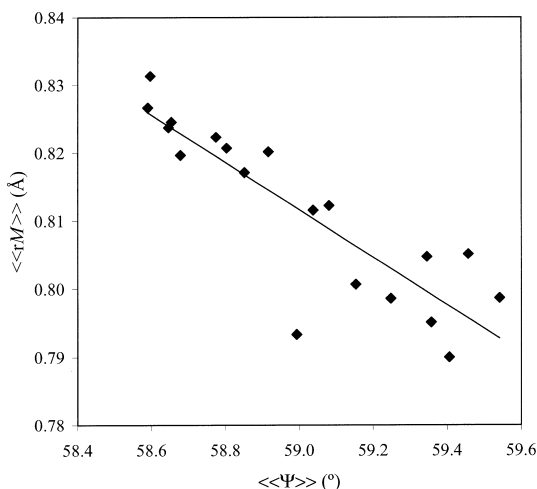
FIG. 11. Average flattening of the octahedra, <<Ψ>>, *versus* the average ionic radius, <<r*M*>> in the *O* sheet. Linear regression, $R^2 = 0.753$.
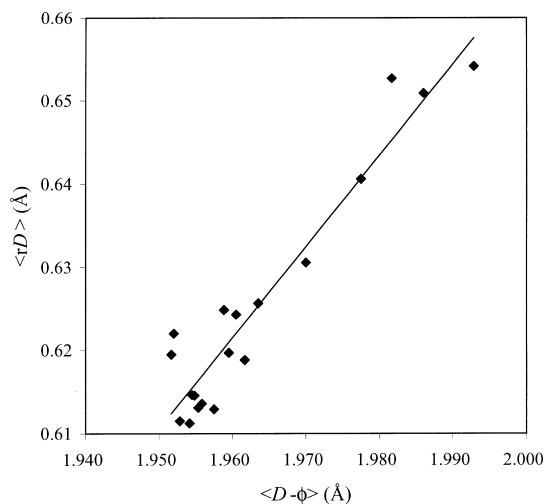
FIG. 12. The variation in mean $D–\phi$ bond length with average ionic radius of the D cations. Linear regression, $R^2 = 0.899$.
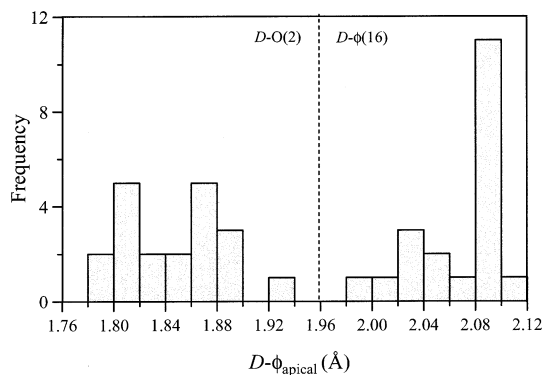
FIG. 13. Bimodal distribution of $D–\phi_{apical}$ bond lengths observed in the $D\phi_6$ octahedra in astrophyllite-group minerals. D–O(2): 1.794(2) to 1.929(8) Å, D–ϕ(16): 1.981(1) to 2.104 Å.
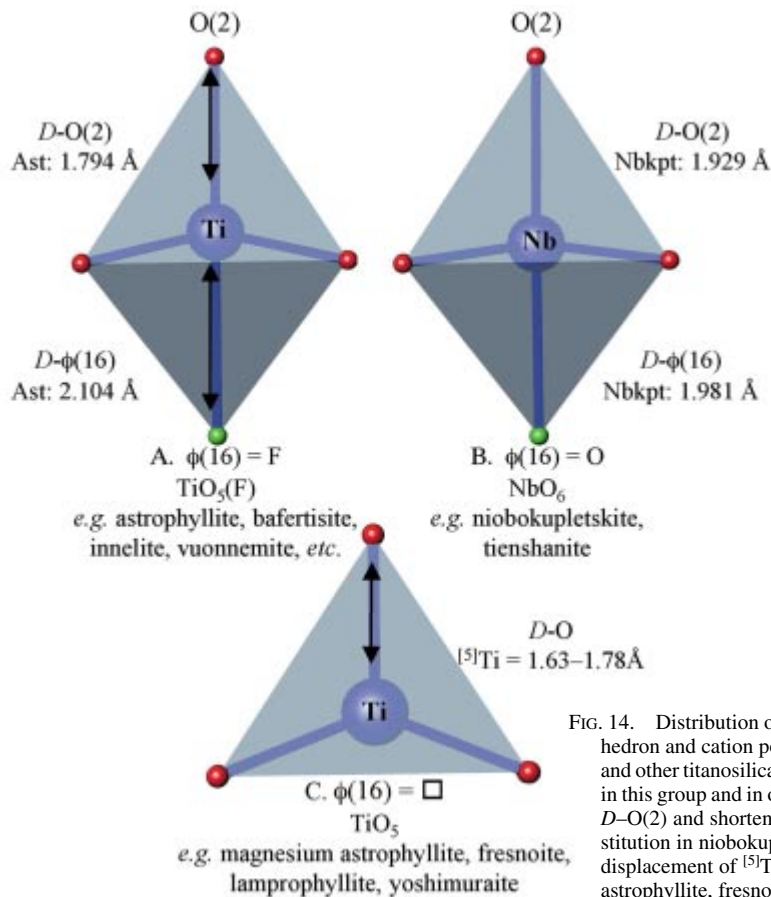
FIG. 14. Distribution of apical bond-lengths in the $D\phi_6$ octahedron and cation position in astrophyllite-group minerals and other titanosilicates. A. Positional displacement of [6]Ti in this group and in other titanosilicates. B. Lengthening of D–O(2) and shortening of D–ϕ(16) due to Nb-for-Ti substitution in niobokupletskite and tienshanite. C. Positional displacement of [5]Ti in titanosilicates such as magnesium astrophyllite, fresnoite, lamprophyllite and yoshimuraite.

charged [6]-coordinated cations (*e.g.*, Ti) occurs where the effective radius of the cation is such that the unstressed *M*–O bond length is $<1/\sqrt{2}$ times the diameter of the oxygen ion. In these cases, the mutual attraction and repulsion effects within the octahedron result in "stressed" bonds, to the point where the anion–anion repulsion has caused the cation–anion bond to be extended beyond its unstressed value. The resultant tension in the O–*M*–O bond length is relaxed by off-center displacement of the cation and relaxation of the O–O edges. The presence of larger cations (*e.g.,* Zr) leads to smaller displacements and longer overall bond-lengths, with a more regular distribution.

In titanosilicates, removal of the long apical anion [*i.e.,* $\phi(16)$ in triclinic astrophyllite-group minerals] results in the formation of [5]-coordinated TiO_5 tetragonal pyramidal units with a shorter titanyl ($Ti=O_{apical}$) bond (1.63 to 1.78 Å), the result of displacement of the Ti atom away from the square plane toward the apex. This shift has been observed in magnesium astrophyllite (monoclinic) [$Ti–O_{apical}$ = 1.755 Å, Shi *et al.* 1998), as well as in other titanosilicates with [5]-coordinated Ti, such as fresnoite ($Ti–O_{apical}$ = 1.6342 Å, Moore & Louisnathan 1969, Markgraf *et al.* 1985), lamprophyllite ($Ti–O_{apical}$ = 1.68 Å, Saf'yanov *et al.* 1983) and yoshimuraite ($Ti–O_{apical}$ = 1.773 Å, McDonald *et al.* 2000), as well as in titanosilicate glasses and melts (*e.g.,* Farges *et al.* 1996a, b).

In astrophyllite-group minerals, the highly asymmetrical nature of the bonding in the $D\phi_6$ octahedra can

be shown to be dependent on the composition of both the *D* and $\phi(16)$ sites. Assuming electronegativities for Ti, Nb and Zr of 1.5, 1.6 and 1.4, respectively, the covalent character of the *D*–O(2) and *D*–$\phi(16)$ bonds in these minerals can be calculated knowing the composition of the $\phi(16)$ site for each composition (Table 8). Calculated characters of the bonds show that the Ti–O(2) bond is 8% more covalent than the Ti–$\phi(16)$ bond, resulting in stronger bonding of the Ti to the O(2) apical oxygen, and thus shorter *D*–O(2) bond lengths relative to *D*–$\phi(16)$. Substitution of Nb for Ti and O for F results in a symmetrical O(2)–Nb–O(16) bond, which is more covalent overall than the asymmetrical O(2)–Ti–F(16) bond observed in Ti-dominant samples. Substitution of Nb for Ti results in a shortening of the *D*–$\phi(16)$ bond and a subsequent lengthening of the *D*–O(2) bond. As such, Nb becomes more centrally located in the octahedron, rather than being displaced along *Z* toward the *O* sheet, as is the case in Ti-dominant minerals of the astrophyllite group (Fig. 14). This is most evident where variations in $<\phi(16)–D–O_{equatorial}>$ and $<O(2)–D–O_{equatorial}>$ bond angles are examined (Fig. 15). Incorporation of Nb at *D* results in an increase of the $<\phi(16)–D–O_{equatorial}>$ angle [range: 80.65(7) to 85.45(31)°] and a concomitant decrease of the $<O(2)–D–O_{equatorial}>$ bond angle [range: 90.04(40) to 99.18(14)°]. This displacement can be estimated by determining the difference in lengths between the *D*–O(2) and *D*–$\phi(16)$ bonds. In Ti-dominant samples, this difference is at a maximum (0.292 Å in MSH20), whereas in Nb-dominant samples, the bond lengths are closer to being equal, and the difference is small (0.052 Å in MSH42, niobokupletskite). The net result of these modifications is a significant decrease in the distortion of the *D* octahedron with increasing Nb-for-Ti substitution (Fig. 16).

A plot of *D*–O(2) *versus* *D*–$\phi(16)$ reveals two distinct trends: (1) increasing *D*–O(2) with decreasing *D*–$\phi(16)$, and (2) increasing *D*–O(2) at constant *D*–$\phi(16)$ (Fig. 17). Plotting the contents of Zr and Nb on this graph shows the first trend to be the result of increasing Nb-for-Ti substitution, and the second the result of Ti-for-Zr substitution. These data confirm the observation that substitution of Nb for Ti decreases the *D*–$\phi(16)$ bond length, whereas lengthening of the *D*–O(2) bond length is due to displacement of the cation within the

TABLE 7. COMPARISON OF (Ti,Nb)–ϕ APICAL BOND-LENGTHS IN ASTROPHYLLITE-GROUP MINERALS AND OTHER TITANOSILICATES AND NIOBOSILICATES

Mineral	[CN]*D*	*D*–O_{apical}	*D*–ϕ_{apical}	Ti SOF
Astrophyllite-group minerals				
[1] Niobokupletskite	[6](Nb,Ti)	1.929	1.981	0.11
Nb-bearing kupletskite	[6](Ti,Nb)	1.887	2.014	0.553
Nb-bearing kupletskite	[6](Ti,Nb)	1.866	2.034	0.624
Kupletskite	[6]Ti	1.794	2.086	1.00
[2] Magnesium astrophyllite	[5]Ti	1.755	--	1.00
Other titanosilicates and niobosilicates				
[3] Bafertisite	[6]Ti	1.823	2.062	1.00
[4] Innelite	[6]Ti	1.90	2.09	1.00
[5] Janhaugite	[6](Ti,Zr)	1.849	2.221	0.67
	[6](Ti,Zr)	1.830	2.268	0.73
[6] Normandite (AF)	[6](Ti,Zr)	1.863	2.064	0.612
[6] Normandite (MSH)	[6](Ti,Nb)	1.781	2.303	0.876
[7] Tienshanite	[6]Ti	1.763	2.200	1.00
	[5](Ti,Nb)	1.824	2.138	0.64
[8] Vuonnemite (K)	[6]Ti	1.734	2.129	1.00
	[6](Nb,Ti)	1.758	2.238	0.165
[9] Barytolamprophyllite	[5]Ti	1.660	--	0.70
[4] Innelite	[5]Ti	1.62	--	1.00
	[5]Ti	1.71	--	1.00
[10] Lamprophyllite	[5]Ti	1.68	--	1.00
[11] Yoshimuraite	[5]Ti	1.773	--	0.69

CN: coordination number, *D*: [5] or [6] Ti, Zr or Nb, SOF: site-occupancy factor.
[1] Piilonen *et al.* (2000), [2] Shi *et al.* (1998), [3] Pen & Sheng (1963), [4] Chernov *et al.* (1971), [5] Annehed *et al.* (1985), [6] Perchiazzi *et al.* (2000, AF: Amdrup Fjord, MSH: Mont Saint-Hilaire), [7] Cooper *et al.* (1998), [8] Ercit *et al.* (1998, K: Kola Peninsula), [9] Rastsvetaeva & Dorfman (1995), [10] Saf'yanov *et al.* (1983), [11] McDonald *et al.* (2000).

TABLE 8. CALCULATED IONIC CHARACTER* OF THE APICAL BOND-LENGTHS IN THE $D\phi_6$ OCTAHEDRA

D cation	O(2)	$\phi(16)$ anion	Ionic character *D*–O(2)	Ionic character *D*–$\phi(16)$
Ti	O^{2-}	F^-	0.393	0.465
Nb	O^{2-}	O^{2-}	0.378	0.378
Zr	O^{2-}	F^-	0.408	0.478

* Ionic character = $1 - e^{-1/4(XA-XB)}$, where XA is the electronegativity of the anion and XB is the electronegativity of the cation. $X(F^-) = 4.0$, $X(O^{2-}) = 3.5$, $X(Ti^{4+}) = 1.5$, $X(Nb^{5+}) = 1.6$, $X(Zr^{4+}) = 1.4$.

octahedron. Although the two bonds change in length relative to each other, the total $O(2)–D–\phi(16)$ bond length along the [001] axis remains unchanged, a reflection of the similar size of the [6]Nb and [6]Ti cations. Samples in which Ti-for-Zr substitution is dominant (indicated by the open diamonds in Fig. 17) display constant $D–\phi(16)$ bond lengths, which are similar to the maximum observed in Nb-free structures. The increase in $D–O(2)$ is due to substitution of the larger Zr cation and expansion of all the bonds in the octahedron (Fig. 12). As a result, the Zr cation is more centrally located within the octahedron, resulting in a more regular distribution of bond lengths, a feature also observed in other zirconium minerals with minimal (Ti,Nb)-for-Zr substitution, such as vlasovite (Voronkov & Pyatenko 1962), wadeite (Tikhonenkov 1964), låvenite (Mellini 1981), sabinaite (McDonald 1996) and eudialyte-group minerals (Johnsen & Grice 1999).

Among the selection of samples studied, the maximum observed Zr content is 1.02 *apfu*, implying that the maximum amount of Zr-for-Ti substitution is ~50%. This limited substitution does not seem to be a function of geochemical factors, such as a lack of Zr in the system; Zr-bearing astrophyllite-group minerals are commonly associated with other Zr-bearing minerals such as catapleiite, elpidite and eudialyte. Instead, the limited substitution of Zr for Ti may be a function of crystal-chemical constraints. For instance, the apical $O(2)$ oxygen of the D octahedron is bonded to $M(1)$, $M(2)$ and $M(3)$ within the O sheet. A lengthening of the $D–O(2)$ bond results in a concomitant shortening of $M(1,2,3)–O(2)$ bonds in the O sheet. This shortening results in increased flattening of the M octahedra and an increase in the O-sheet dimensions that cannot be accommodated by structural change in the H sheet. Incorporation of more than 1.00 *apfu* Zr into the astrophyllite structure may require (1) extensive ordering of Ti and Zr, or (2) modifications (*i.e.,* expansion) of the H sheet

not be possible in the $P\bar{1}$, $C2/c$ or $A2$ configurations recognized in the astrophyllite group to date.

With the exception of seidozerite, zircophyllite and the Fe-dominant analogue zircophyllite, Zr in zirconosilicates occurs in isolated [6]- to [8]-coordinated polyhedra, forming a three-dimensional network with SiO_4 tetrahedra. Zirconium-bearing polyhedra display a nega-
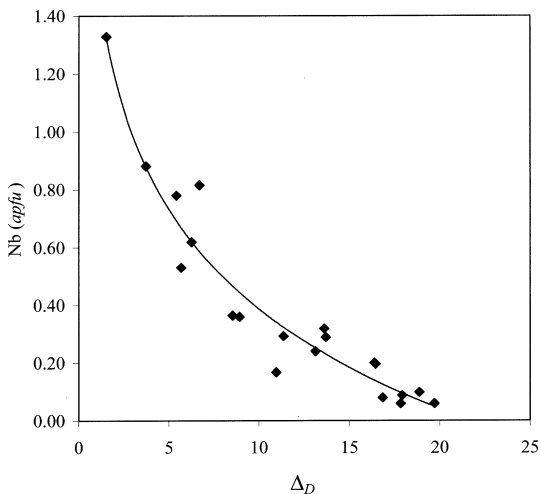
FIG. 16. The effects of Nb-for-Ti substitution on the distortion index (Δ) of the D octahedron. $y = -0.4976 \ln(x) + 1.5318$, $R^2 = 0.9314$.
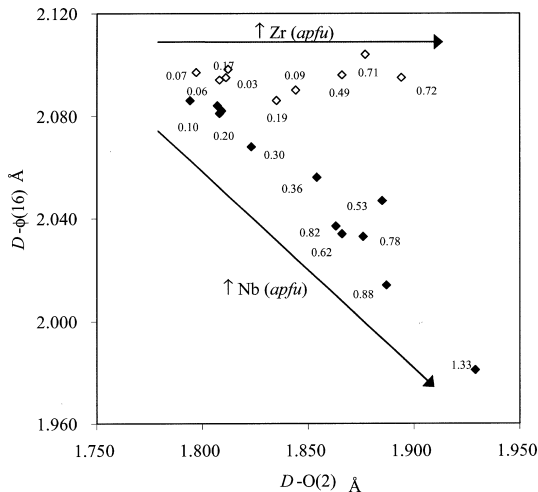
FIG. 17. Control by content of high field-strength elements on apical bond-lengths in the $D\phi_6$ octahedra. Open diamonds represent Zr contents (*apfu*). Closed diamonds represent Nb contents (*apfu*).

FIG. 15. Distribution of $O(2)–D–O_{equatorial}$ and $\phi(16)–D–O_{equatorial}$ bond angles in the $D\phi_6$ octahedra.

tive tendency toward polymerization (Pyatenko & Voronkov 1978). On the other hand, Ti polyhedra in titanosilicates tend to polymerize, most commonly *via* apices and even *via* common edges. In fact, natural examples of crystal structures with discrete, isolated Ti octahedra are rare, which may suggest that these structures are metastable (Pyatenko & Voronkov 1978). In cases where there is substantial Ti and Zr in a mineral, the two cations tend to partially or completely order (Pyatenko & Voronkov 1978; *e.g.*, rosenbuschite: Shibaeva *et al.* 1964, sabinaite: McDonald 1996). Complete solid-solution series between minerals with Ti- and Zr-dominant end-members have not been found. In minerals of the astrophyllite group, owing to the presence of substantial concentrations of Nb, it was not possible to effectively evaluate the degree of order of Ti and Zr.

The T sites

There are four crystallographically unique tetrahedral sites in the structure, labeled $T(1)$ through $T(4)$. The $T(1)$ and $T(4)$ sites are each coordinated by one bridging (*br*) [O(13) and O(14), respectively] and three nonbridging (*nb*) oxygen atoms [$T(1)$: O(1), O(11) and O(15), $T(4)$: O(7), O(9) and O(12)]. The $T(1)$ and $T(4)$ tetrahedra share corners with the $D\phi_6$ octahedra *via* non-

bridging O, forming $T(1,4)–O_{nb}–D$ linkages perpendicular to [100]. The $T(2)$ and $T(3)$ tetrahedra are each coordinated by three bridging and one non-bridging oxygen atoms [$T(2)$: bridging O(8), O(10) and O(13), non-bridging: O(3); $T(3)$: bridging: O(8), O(10), and O(14), nonbridging: O(6)]. The $T(2)$ and $T(3)$ tetrahedra alternate along the length of the chain, forming O(8)–$T(2)$–O(10)–$T(3)$ linkages parallel to [100]. $T(1)$ and $T(4)$, the branches of the chain, are linked *via* bridging oxygen atoms to the main chain by O(13) and O(14). Bond-valence sums to the four T sites range from 3.838 to 4.260 *vu*.
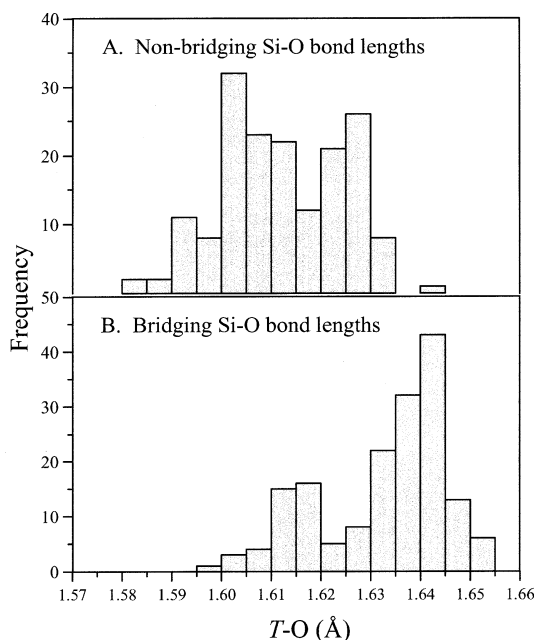
Bond lengths in all four tetrahedra range from 1.588(3) to 1.654(8) Å, consistent with values expected for essentially Al-free tetrahedra. The distribution of T–O bond lengths in the samples studied is shown in Figure 18. In general, the length of $T–O_{br}$ bonds exceeds that of $T–O_{nb}$ bonds (averages: 1.598 and 1.585 Å respectively), a feature observed in all silicates because of the presence of a second Si atom linked to the O^{2-} of the Si–O bond, which results in repulsion of the two Si^{4+} cations, weakening, and therefore elongating, the Si–O_{br} bond (Brown & Gibbs 1969, Liebau 1985). Similarly, O–Si–O bond angles should decrease in magnitude such that $O_{nb}–Si–O_{nb}$ exceeds $O_{br}–Si–O_{nb}$ (Liebau 1985). In astrophyllite-group minerals, O–Si–O bond angles range from 104.83(62) to 112.74(53)°, yet the trend deviates slightly from that expected because the $D\phi_6$ octahedron has characteristics more similar to those of a SiO$_4$ tetrahedron (*i.e*,. part of the anionic framework) rather than those belonging to the O sheet; O_{nb}–Si–O_{br} bond angles that include anions of the $D\phi_6$ octahedron are similar in magnitude to O_{br}–Si–O_{br} bonds angles. Five distinct populations of O–Si–O bond angles are observed, decreasing in magnitude in the order I > II > III > IV > VI (Table 9):

I. $O_{nb}–Si–O_{nb}$, where O_{nb} are from the O sheet and $D\phi_6$ only [*e.g.*, O(1)–Si(1)–O(15)],

II. $O_{nb}–Si–O_{br}$, where O_{nb} is from the O sheet only [*e.g.*, O(1)–Si(1)–O(13)],

III. $O_{nb}–Si–O_{nb}$, where O_{nb} are from the $D\phi_6$ octahedron [*e.g.*, O(11)–Si(1)–O(15)],

IV. $O_{br}–Si–O_{br}$ [*e.g.* O(8)–Si(3)–O(10)],

FIG. 18.   Distribution of T–O bond distances in the H sheet. A: Non-bridging Si–O bonds (Å). B: Bridging Si–O bonds (Å).

TABLE 9.   O–T–O BOND ANGLES (°) IN ASTROPHYLLITE-GROUP MINERALS

Type		Average	Median	Mode	Range
I	$O_{nb}–Si–O_{nb}$	111.4	111.4	111.2	110.8–111.8
II	$O_{nb}–Si–O_{br}$	111.3	111.3	111.6	110.1–113.1
III	$O_{nb}–Si–O_{nb}$	110.5	110.5	110.5	109.5–112.3
IV	$O_{br}–Si–O_{br}$	107.8	106.6	106.4	104.9–112.0
V	$O_{br}–Si–O_{nb}$	105.8	105.9	106.2	104.8–106.9

I O_{nb} are from the O-sheet and $D\phi_6$ only [*e.g.*, O(1)–Si(1)–O(15)]
II O_{nb} is from the O-sheet only [*e.g.*, O(1)–Si(1)–O(13)]
III O_{nb} are from the $D\phi_6$ octahedron [*e.g.*, O(11)–Si(1)–O(15)]
IV O_{br} are from the T tetrahedra only [*e.g.*, O(8)–Si(3)–O(10)]
V O_{nb} is from the $D\phi_6$ octahedron [*e.g.*, O(13)–Si(1)–O(11)]

V. O_{br}–Si–O_{nb}, where O_{nb} is from the $D\phi_6$ octahedron [*e.g.*, O(13)–Si(1)–O(11)].

A similar trend is observed with *T*–O–(*T*,*D*,*M*) bond angles. *T*–O–*M* angles are characteristically smaller than Si–O–Si angles, a result once again of the greater repulsion of Si atoms compared to that encountered by larger, lower-valence *M* cations such as Mn^{2+} or Fe^{2+} (Liebau 1985). *T*–O–*M* angles in minerals of this group range from 117.36(23) to 124.28(24)° (average: 121.1°), significantly smaller than the *T*–O–*T* angles, which range from 138.14(30) to 144.35(43)°, with an average, 141.1°, close to the ideal angle of 139° for a strain-free Si–O–Si bond (Liebau 1985; Fig. 19). Two populations of *T*–O–*T* bond angles are observed: (1) those of the main chain of tetrahedra, *T*(2)–O–*T*(3), with an average value of ~139°, and (2) those of tetrahedra on the branches of the chain, *T*(1)–O–*T*(2) and *T*(3)–O–*T*(4), with a slightly higher average value of 143° (Fig. 19), suggesting slightly increased strain on the *T*(1) and *T*(4) tetrahedra. *T*–O–*D* linkages show a range of bond angles between 140.04(16) and 145.92(72)° (average: 142.3°), comparable to *T*–O–*T* linkages between tetrahedra of the main chain [*T*(2) and T(3)] and the outer branches [*T*(1) and *T*(4)]. Again, we show that the $D\phi_6$ octahedron shares close affinities with SiO_4 tetrahedra and not with octahedra normally considered to be part of the cationic structure (*i.e.*, the *O* sheet).

Large differences in basal bond-lengths are observed in the *T*(1) and *T*(4) tetrahedra owing to (1) displacement of the *T* cation toward the $D\phi_6$ octahedron, and (2) tilting of the tetrahedra out of the (001) plane. As a result, *T*(1)–O(13) and *T*(4)–O(14) are the longest *T*–O bonds observed in the structure [range: 1.607(9) to 1.649(3) Å, average: 1.640 and 1.633 Å, respectively). In order to maintain a mean *T*–O bond valence of ~1.5 *vu* in the tetrahedron and a BVS for the Si of ~4.00 *vu*, an increase in a particular bond-length in the tetrahedron must be accompanied by a decrease in length of the remaining bonds (Robinson 1963). Consequently, *T*(1)–O(11,15) and *T*(4)–O(9,12) are unusually short, ranging from 1.585(9) to 1.615(3) Å, with an average of 1.603 Å, 0.017 Å shorter than the ideal Si–O bond length of 1.62 Å (Liebau 1985). *T*(1) and *T*(4) are, on average, the most distorted tetrahedra in the structure [$\Delta T(1)_{ave}$: 1.045, $\Delta T(4)_{ave}$: 0.773]. Shortening of these bonds may also be the result of a displacement of the Si cation due to tilting of the *T*(1) and *T*(4) tetrahedra toward the $D\phi_6$ octahedron. Similarly, *T*(2)–O(13) and *T*(3)–O(14) bonds also are short (average: 1.614 and 1.615 Å, respectively) to maintain a BVS of 2.00 *vu* at the bridging oxygen atoms O(13) and O(14).

LATERAL FIT OF THE *H* AND *O* SHEETS

In astrophyllite-group minerals, there is a mismatch in size between the *O* and *H* sheets, similar to that observed between the sheets of tetrahedra (*T*) and octahedra (O) in micas (Bailey 1984). In true micas, the lateral

dimensions of the *T* sheet are larger than those of the adjacent *O* sheets. The mismatch between the *T* and *O* sheets is generally compensated for by the rotation, tilting and elongation of the tetrahedra, along with flattening and rotation of the octahedra. In minerals of the astrophyllite group, a similar response is observed. However, the composition of the *O* sheet here is quite different from that of a mica; specifically, it is dominated by relatively large Mn^{2+} cations ($r^{[6]}Mn^{2+}$: 0.83 Å) rather than smaller cations such as Fe^{2+} (0.78 Å), Mg (0.72 Å) and Al (0.54 Å; ionic radii from Shannon 1976). Similarly, the presence of the $D\phi_6$ octahedron in the *H* sheet results in a larger *H* sheet than in *T* sheets in a mica. As a result, the methods by which the structure
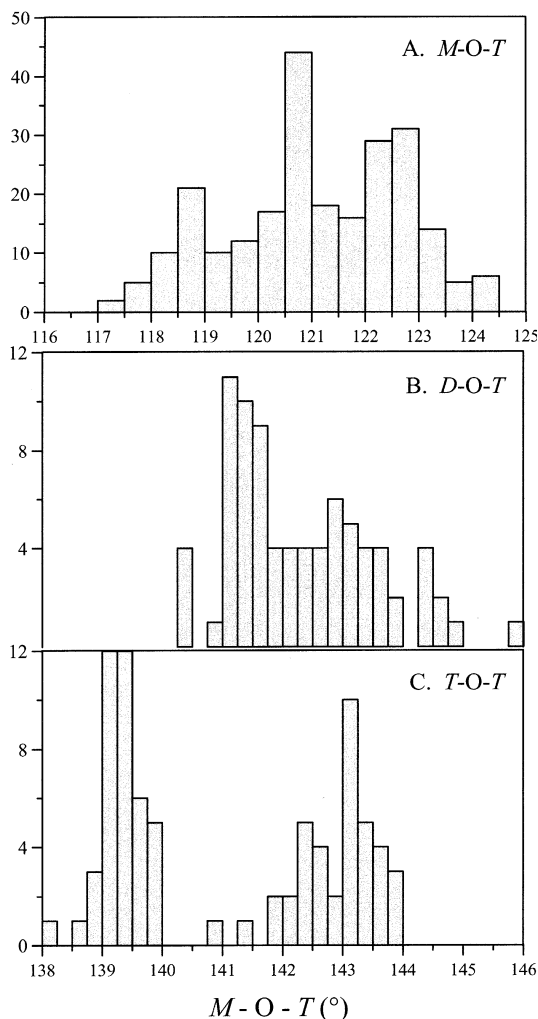

FIG. 19. Distribution of *M*–O–Si bond angles; A. *M*–O–*T*, B. *D*–O–*T*, C. *T*–O–*T*.

adapts to the mismatch are somewhat different than those encountered in micas. The dominant mechanisms by which lateral fit of H and O sheets occurs are: (1) trigonal distortion of the O-sheet octahedra, namely isometric flattening and counter-rotation, and (2) rotation, tilting and elongation of tetrahedra in the H and T sheets.

Isometric flattening of the octahedra is one of the primary ways by which the lateral dimensions of *the* O sheet increase. Flattening angles in the O-sheet octahedra range from 58.4 to 59.7°, similar to other 2:1 phyllosilicates, which commonly have Ψ values in the range 58 to 61° (Bailey 1984). Flattening angles in astrophyllite-group minerals are most similar to those in Fe^{2+}-bearing samples of the biotite series (58 to 59°), a result of their greater similarity in O-sheet composition, in contrast to Al- and Mg-bearing species such as muscovite and phlogopite ($\Psi = 60$ to 61°; Bailey 1984). Flattening of octahedra in the O sheet is dependent on the size of the M cation, such that increased rM results in decreased flattening of the octahedra (Fig. 20). The increase in rM is due to increased Mn-for-Fe^{2+} substitution (Fig. 19), whereas in members of the biotite series, the dominant substitution is $Fe^{2+} \Leftrightarrow Mg$ (Fig. 20; Shabani 1999). The larger Ψ angles in minerals of the astrophyllite group, compared to those of the biotite series, which have substantially smaller values for rM, are due to the larger dimensions of the H sheet to which the O sheet must attach. The flattening of octahedra is further complicated by the presence of the $D\phi_6$ octahedron within the H sheet. The apical O(2) oxygen of the $D\phi_6$ octahedron is bonded to three octahedra within the
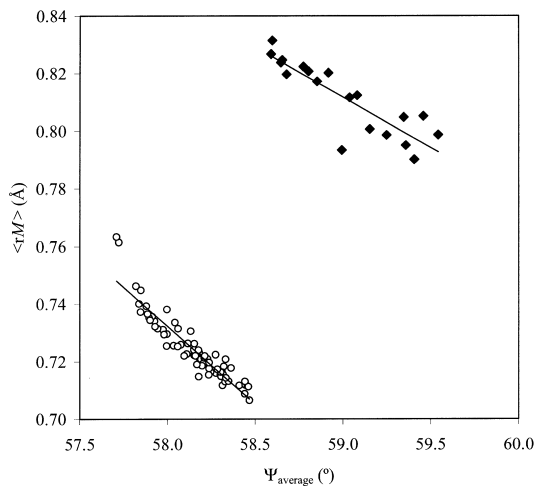

FIG. 20.   Average flattening of octahedra ($\Psi_{average}$) of the O sheet *versus* the average ionic radius (rM) in astrophyllite-group minerals (closed diamonds; linear regression: $R^2 = 0.753$) and members of the biotite series [open circles; Shabani (1999); linear regression: $R^2 = 0.869$].

O sheet, $M(1)$, $M(2)$ and $M(3)$. Bond lengths to O(2) from $M(2)$ and $M(3)$ are the longest observed in the O sheet, a response to the presence of Nb or Zr at D in order to satisfy bond-valence requirements at the O(2) oxygen [$M(2)$–O(2): 2.230 to 2.267 Å, $M(3)$–O(2): 2.209 to 2.246 Å). Conversely, $M(1)$–O(2) bond lengths are short (range: 2.137 to 2.189 Å). This lengthening and shortening of M–O(2) bonds result in a corrugated appearance of the O sheet around O(2) and the $D\phi_6$ octahedron.

Reduction in the lateral dimensions of the H sheet occurs by rotation of adjacent tetrahedra in opposite directions in the (001) plane. In an ideal six-membered ring of SiO_4 tetrahedra, the angle O_{br}–O_{br}–O_{br} of the basal oxygen atoms is 120°; deviation from this value is the result of rotation of the tetrahedra (α). Angles of rotation in true micas range from 1.4 to 11.0° in trioctahedral species, and from 6.0 to 19.1° in dioctahedral species (Bailey 1984). In minerals of the astrophyllite group, O_{br}–O_{br}–O_{br} angles range from 114.76(16) to 125.64(16)°, with an average of 119.6°, close to the ideal 120°, and rotation angles of the tetrahedra (α) range from 0 to 2.82° (average: 1.24°). Figure 21 shows the relative rotation of the tetrahedra in the H sheet. As with micas, rotation of adjacent tetrahedra in minerals of the astrophyllite group occurs in opposite directions. The α values in these minerals are insignificant in terms of altering the lateral dimensions of the H sheet in order to compensate for the misfit with the O sheet, and another mechanism must be considered.

Isometric flattening and counter-rotation of the O-sheet octahedra, for example, result in elongation of the edges of the octahedra in an attempt to compensate for the mismatch between the O and H sheets. In order for the lateral dimensions of the H sheet to match these elongate edges, the tetrahedra are thickened along [001] by elongation of Si–O_{apical} bond lengths and widening of O_{apical}–Si–O_{basal} bond angles, and are tilted out of the (001) plane. The ideal tetrahedral angle, $\tau = O_{apical}$–Si–O_{basal}, of 109.47° can be increased by elongation and decreased by shortening of Si–O_{apical} bonds (Bailey 1984). In astrophyllite-group minerals, τ angles range from 110.8 to 111.8°, indicating ~2% thickening of the tetrahedra in the [001] direction, comparable to that observed in true micas (τ angles range from 108 to 114°, Bailey 1984). The $T(1)$ and $T(4)$ tetrahedra show increased thickening (average: 111.76 and 111.79°, respectively) compared to $T(2)$ and $T(3)$ (average: 111.34 and 111.65°, respectively), the result of increased tilting out of the (001) plane of the $T(1)$ and $T(4)$ tetrahedra.

The principal mechanism by which lateral misfit of the sheets may be reduced is by tilting of the tetrahedra out of the (001) plane such as to reduce the a and b dimensions of the H sheet. Tilting of the $T(1)$ and $T(4)$ tetrahedra brings the apices of the tetrahedra toward the O(2) apex of the $D\phi_6$ octahedron, whereas $T(2)$ and $T(3)$

are tilted in opposite directions, toward each other and the main SiO_4 chain of the *H* sheet. The presence of the larger $D\phi_6$ octahedra results in increased thickening of the *T*(1) and *T*(4) tetrahedra (as discussed above) and increased tilting; *T*(1) and *T*(4) are tilted a substantial amount more out of the (001) plane (average: 6.80 and 7.09°, respectively) than *T*(2) and *T*(3) (average: 2.06 and 0.87°, respectively), adding to the strongly corrugated appearance of the *HOH* layers.

Conclusions

The complex chemical compositions exhibited by astrophyllite-group minerals result in a wide range of structural variations. The relations between composition and crystal structure are summarized here:

1) Members of the astrophyllite group are heterophyllosilicates and are intermediate members of a polysomatic (or homologous) series with perraultite and mica as the end-member structures. The structure consists of two composite sheets stacked along [001] in a 2:1 ratio, resulting in a layered *HOH* structure.

2) The interlayer in triclinic members of the group consists of two crystallographically distinct cation sites, *A* and *B*, whereas three distinct sites occur in kupletskite-*Ma2b2c*, *A*(1), *A*(2) and *B*. The [13]*A* site(s) predominantly contains K, with minor incorporation of Rb, Cs and Na, and up to 15% vacancies. In many cases, the *A* site is positionally disordered, and there is smearing of electron density in the (001) plane. The [10]*B* site is host to predominantly Na, with up to 40% occupancy by Ca.

3) The sheet of octahedra consists of four crystallographically distinct MO_6 octahedra, designated *M*(1) through *M*(4), in a 2:2:2:1 ratio, respectively, and contains Mn, Fe^{2+}, Fe^{3+}, Na, Mg and Zn as the principal cations. The *M*(1) octahedron is the largest and least distorted within the *O* sheet and contains significant Na. The *M*(2) octahedron is highly distorted and forms zigzag chains parallel to *a*. The *M*(3) and *M*(4) sites form a composite chain parallel to *a* and are occupied by Mn, Fe^{2+}, Fe^{3+}, Mg and Zn.

4) The *H* sheet (heterogeneous sheet) has the ideal composition $[(Ti,Nb,Zr)Si_4O_{12}]^{4-}$ and consists of open-branched *zweier* [100] single chains of $[Si_4O_{12}]^{8-}$, which are cross-linked by corner-sharing $D\phi_6$ octahedra in triclinic species and kupletskite-*Ma2b2c*, and DO_5 polyhedra in magnesium astrophyllite, where *D* = Nb, Ti, Zr. Substitution of Nb for Ti at *D* results in lengthening of the *D*–O(2) bond, shortening of the *D*–ϕ(16) bond, and positional displacement of the *D* cation toward the center of the octahedron, with an overall decrease in the distortion index, Δ. Substitution of Zr for Ti at *D* results in an increase in all *D*–ϕ bond lengths and a simultaneous decrease in Δ. Crystallographic restrictions limit the maximum Zr content to approximately 1 *apfu* (50% occupancy of *D*).

5) There are four tetrahedrally coordinated sites in the structure, designated *T*(1) through *T*(4). All four sites contain dominantly Si, with only minor incorporation of Al. *T*(1) and *T*(4) are located on the branches of the *zweier* single chains and share oxygen atoms with the $D\phi_6$ octahedron, whereas *T*(2) and *T*(3) are located in the central portion of the chain and share only apical oxygen atoms with the *O* sheet.

6) There is a lateral misfit between the *H* and *O* sheets, similar to that observed in 2:1 phyllosilicates. Lateral misfit increases with increasing Mn-for-Fe and Zr-for-(Ti,Nb) substitution. Lateral fit of the *H* and *O* sheets in the structure is accomplished by tilting of the tetrahedra out of the (001) plane, thickening or elongation of the tetrahedra along [001], and flattening of the *O*-sheet octahedra.

References

ANNEHED, H., FÄLTH, L. & RAADE, G. (1985): The crystal structure of janhaugite, a sorosilicate of the cuspidine family. *Neues Jahrb. Mineral., Monatsh*, 7-18.

BAILEY, S.W. (1984): Crystal chemistry of the true micas. *In* Micas (S.W. Bailey, ed.). *Rev. Mineral.* **13**, 13-60.

BALIĆ-ŽUNIĆ, T. & MAKOVICKY, E. (1996): Determination of the centroid or 'the best centre' of a coordination polyhedron. *Acta Crystallogr.* **B52**, 78-81.

_____ & VICKOVIĆ, K. (1996): IVTON. A program for the calculation of geometrical aspects of crystal structures and some crystal chemical applications. *J. Appl. Crystallogr.* **29**, 305-306.

BRESE, N.E. & O'KEEFFE, M. (1991): Bond-valence parameters for solids. *Acta Crystallogr.* **B47**, 192-197.

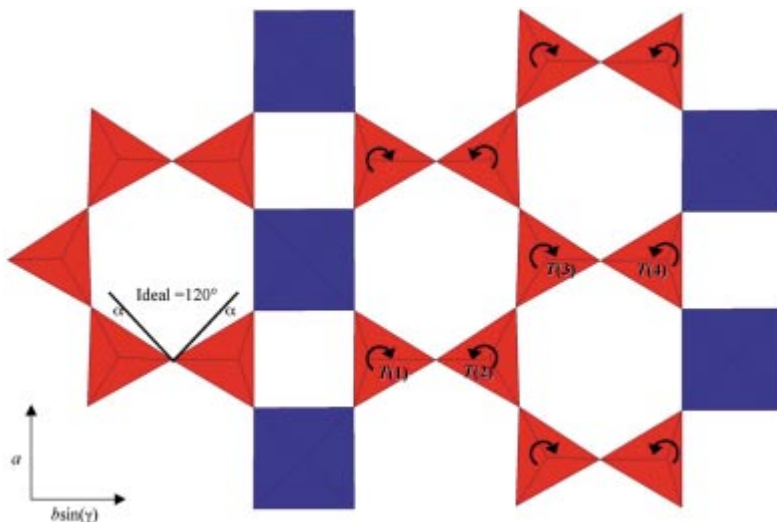BROWN, G.E. & GIBBS, G.V. (1969): Oxygen coordination and the Si–O bond. *Am. Mineral.* **54**, 1528-1539.

FIG. 21.   Rotation of tetrahedra (arrows) in the *H* sheet. The ideal O_{br}–O_{br}–O_{br} angle is 120° (exaggerated in order to show α angles). Rotation angles of tetrahedra (α) range from 0 to 2.82° (average: 1.24°). SiO_4 tetrahedra: orange; $D\phi_6$ octahedra: blue.

BROWN, I.D. & SHANNON, R.D. (1973): Empirical bond-strength – bond-length curves for oxides. *Acta Crystallogr.* **A29**, 266-282.

BRUKER ANALYTICAL X-RAY SYSTEMS (1997): XPREP – Data preparation and Reciprocal Space Exploration.

CHERNOV, A.N., ILYUKHIN, V.V., MAKSIMOV, B.A. & BELOV, N.V. (1971): Crystal structure of innelite, Na_2Ba_3 $(Ba,K,Mn)(Ca,Na)Ti(TiO_2)_2[Si_2O_7]_2(SO_4)_2$. *Sov. Phys. Crystallogr.* **16**(1), 65-69.

CHRISTIANSEN, C.C., JOHNSEN, O. & STÅHL, K. (1998): Crystal structure of kupletskite from the Kangerdlugssuaq intrusion, East Greenland. *Neues Jahrb. Mineral., Monatsh.*, 253-264.

————, MAKOVICKY, E. & JOHNSEN, O. (1999): Homology and typism in heterophyllosilicates: an alternative approach. *Neues Jahrb. Mineral., Abh.* **175**, 153-189.

COOPER, M.A., HAWTHORNE, F.C. & GREW, E.S. (1998): Refinement of the crystal structure of tienshanite: short-range-order constraints on chemical composition. *Can. Mineral.* **36**, 1305-1310.

CROMER, D.T. & LIBERMAN, D. (1970): Relativistic calculation of anomalous scattering factors for X rays. *J. Chem. Phys.* **53**, 1891-1898.

ERCIT, T.S., COOPER, M.A. & HAWTHORNE, F.C. (1998): The crystal structure of vuonnemite, $Na_{11}Ti^{4+}Nb_2(Si_2O_7)_2$ $(PO_4)_2O_3(F,OH)$, a phosphate-bearing sorosilicate of the lomonosovite group. *Can. Mineral.* **36**, 1311-1320.

EVANS, R.J. (2000): *OCTAHEDRON. A program for calculation of octahedral flattening angles and counter rotations*. Dept. of Phyics, Univ. Ottawa, Ottawa, Canada.

FARGES, F., BROWN, G.E., JR., NAVROTSKY, A., GAN, HAO & REHR, J.J. (1996b): Coordination chemistry of Ti(IV) in silicate glasses and melts. II. Glasses at ambient temperature and pressure. *Geochim. Cosmochim. Acta* **60**, 3039-3053.

————, ———— & REHR, J.J. (1996a): Coordination chemistry of Ti(IV) in silicate glasses and melts. I. XAFS study of titanium coordination in oxide model compounds. *Geochim. Cosmochim. Acta* **60**, 3023-3038.

FERRARIS, G. (1997): Polysomatism as a tool for correlating properties and structure. *In* Modular Aspects of Minerals. *Eur. Mineral. Union, Notes in Mineralogy* **1**, 275-295.

————, IVALDI, G., KHOMYAKOV, A.P., SOBOLEVA, S.V., BELLUSO, E. & PAVESE, A. (1996): Nafertisite, a layer titanosilicate member of a polysomatic series including mica. *Eur. J. Mineral.* **8**, 241-249.

————, ————, PUSHCHAROVSKY, D.YU., ZUBKOVA, N.V. & PEKOV, I.V. (2001): The crystal structure of delindeite, $Ba_2\{(Na,K,\square)_3(Ti,Fe)[Ti_2(O,OH)_4Si_4O_{14}]$ $(H_2O,OH)_{12}\}$, a member of the mero-plesiotype bafertisite series. *Can. Mineral.* **39**, 1306-1316.

HAWTHORNE, F.C. (1981): Crystal chemistry of the amphiboles. *In* Amphiboles and Other Hydrous Pyriboles – Mineralogy (D.R. Veblen, ed.). *Rev. Mineral.* **9A**, 1-102.

JOHNSEN, O. (1996): TEM observations and *X*-ray powder data on lamprophyllite polytypes from Gardiner Complex, East Greenland. *Neues Jahrb. Mineral., Monatsh.*, 407-417.

_____ & GRICE, J.D. (1999): The crystal chemistry of the eudialyte group. *Can. Mineral.* **37**, 865-890.

KHALILOV, A.D. (1990): Refinement of the crystal structure of β-lomonosovite from the Lovozero alkaline massif. *Mineral. Zh.* **12**(5), 10-18 (in Russ.).

LIEBAU, F. (1985): *Structural Chemistry of Silicates: Structure, Bonding and Classification*. Springer-Verlag, Berlin, Germany.

MA ZHESHENG, LI GUOWU, SHI NICHENG, ZHOU HUYUN, YE DANIAN & PUSHCHAROVSKY, D.YU. (2000): Structure refinement of astrophyllite. *Sci. China* **30D**, 399-406 (in Chinese).

MAKOVICKY, E. & BALIĆ-ŽUNIĆ, T. (1998): New measure of distortion for coordination polyhedra. *Acta Crystallogr.* **B54**, 766-773.

MARKGRAF, S.A., SHARMA, S.K., BHALLA, A.S. & NEWNHAM, R.E. (1985): X-ray structure refinement and pyroelectric investigation of fresnoite, $Ba_2TiSi_2O_8$. *Ferroelectrics* **62**, 17-26.

MCDONALD, A.M. (1996): The crystal structure of sabinaite, $Na_4Zr_2TiO_4(CO_3)_4$. *Can. Mineral.* **34**, 811-815.

_____, GRICE, J.D. & CHAO, G.Y. (2000): The crystal structure of yoshimuraite, a layered Ba–Mn–Ti silicophosphate, with comments on five-coordinated Ti^{4+}. *Can. Mineral.* **38**, 649-656.

MEGAW, H.D. (1968a): A simple theory of the off-centre displacement of cations in octahedral environments. *Acta Crystallogr.* **B24,** 149-153.

_____ (1968b): The thermal expansion of interatomic bonds, illustrated by experimental evidence from certain niobates. *Acta Crystallogr.* **A24**, 589-604.

MELLINI, M. (1981): Refinement of the crystal structure of låvenite. *Tschermaks Mineral. Petrogr. Mitt.* **28**, 99-112.

_____ & MERLINO, S. (1979): Refinement of the crystal structure of wöhlerite. *Tschermaks Mineral. Petrogr. Mitt.* **26**, 109-123.

MOORE, P.B. & ARAKI, T. (1977): Samuelsonite: its crystal structure and relation to apatite and octacalcium phosphate. *Am. Mineral.* **62**, 229-245.

_____ & LOUISNATHAN, J. (1969): The crystal structure of fresnoite, $Ba_2(TiO)[Si_2O_7]$. *Z. Kristallogr.* **130**, 438-448.

ONDIK, H. & SMITH, D. (1962): Interatomic distances in inorganic compounds. *In* International Tables for X-Ray Crystallography. III. Interatomic and Interionic Distances (C.H. MacGillavry & G.D. Rieck, eds.). Kynoch Press, Birmingham, U.K. (257-274).

PEN, Z.Z. & SHENG, T.C. (1963): Crystal structure of bafertisite, a new mineral from China. *Sci. Sinica* **12**, 278-280 (in Russ.).

PENG, C.C. & MA, C.S. (1963): Crystal structure of astrophyllite and a new type of band silicate radical. *Sci. Sinica* **12**, 272-276 (in Russ.).

PERCHIAZZI, N., MCDONALD, A.M., GAULT, R.A., JOHNSEN, O. & MERLINO, S. (2000): The crystal structure of normandite and its crystal-chemical relationships with låvenite. *Can. Mineral.* **38**, 641-648.

PIILONEN, P.C., LALONDE, A.E., MCDONALD, A.M. & GAULT, R.A. (2000): Niobokupletskite, a new astrophyllite-group mineral from Mont Saint-Hilaire, Quebec, Canada: description and crystal structure. *Can. Mineral.* **38**, 627-639.

_____, _____, _____, _____ & LARSEN, A.O. (2003): Insights into the astrophyllite group. I. Nomenclature, composition and development of a standardized general formula. *Can. Mineral.* **41**, 1-26.

_____, MCDONALD, A.M. & LALONDE, A.E. (2001): Kupletskite polytypes from the Lovozero massif, Kola Peninsula, Russia: kupletskite-1*A* and kupletskite-*Ma*2*b*2*c*. *Eur. J. Mineral.* **13**, 973-984.

PYATENKO, YU.A. & VORONKOV, A.A. (1978): Comparative crystal-chemical functions of titanium and zirconium in mineral structures. *Int. Geol. Rev.* **20**, 1050-1058.

RASTSVETAEVA, R.K. & DORFMAN, M.D. (1995): Crystal structure of Ba-lamprophyllite in the isomorphous lamprophyllite–barytolamprophyllite series. *Kristallografiya* **40**, 1026-1029 (in Russ.).

ROBINSON, E.A. (1963): Characteristic vibrational frequencies of oxygen compounds of silicon, phosphorus and chlorine: correlation of stretching frequencies and force constants with bond lengths and bond orders. *Can. J. Chem.* **41**, 3021-3033.

ROBINSON, K., GIBBS, G.V. & RIBBE, P.H. (1971): Quadratic elongation: a quantitative measure of distortion in coordination polyhedra. *Science* **172**, 567-570.

SAF'YANOV, Y.N., VASIL'EVA, N.O., GOLOVACHEV, V.P., KUZ'MIN, É.A. & BELOV, N.V. (1983): Crystal structure of lamprophyllite. *Sov. Phys. Crystallogr.* **28**, 207-209.

SHABANI, A.A.T. (1999): *Mineral Chemistry and Mössbauer Spectroscopy of Micas from Granitic Rocks of the Canadian Appalachians*. Ph.D. thesis, Univ. Ottawa, Ottawa, Canada.

SHANNON, R.D. (1975): Systematic studies of interatomic distances in oxides. *In* The Physics and Chemistry of Minerals and Rocks (R.G.J. Strens, ed.). John Wiley & Sons, New York. N.Y.

_____ (1976): Revised effective ionic radii and systematic studies of interatomic distances in halides and chalcogenides. *Acta Crystallogr.* **A32**, 751-767.

SHELDRICK, G.M. (1993): SHELXL-93. Program for the refinement of crystal structures. University of Göttingen, Göttingen, Germany.

SHI NICHENG, MA ZHESHENG, LI GUOWU, YAMNOVA, N.A. & PUSHCHAROVSKY, D.YU. (1998): Structure refinement of monoclinic astrophyllite. *Acta Crystallogr.* B**54**, 109-114.

SHIBAEVA, R.P., SIMONOV, V.I. & BELOV, N.V. (1964): Crystal structure of the Ca, Na, Zr, Ti silicate rosenbuschite, $Ca_{3.5}Na_{2.5}Zr(Ti,Mn,Nb)[Si_2O_7]_2F_2O(F,O)$. *Sov. Phys. Crystallogr.* **8**, 406-413.

SIMONOV, V.I. & BELOV, N.V. (1960): The determination of the structure of seidozerite. *Sov. Phys. Crystallogr.* **4**, 146-157.

TAYLOR, R. (1999): *The Crystal Chemistry of Amphiboles from Mont Saint-Hilaire, Québec*. B.Sc. thesis, Laurentian University, Sudbury, Canada.

TIKHONENKOV, I.P. (1964): Zirconium minerals. *In* Geochemistry, Mineralogy and Genetic Types of Deposits of Rare Elements. II. Mineralogy of Rare Elements. Izd-vo Nauka, Moscow, Russia.

VORONKOV, A.A., ZHDANOVA, T.A. & PYATENKO, YU.A. (1974): Refinement of the structure of vlasovite $Na_2ZrSi_4O_{11}$ and some characteristics of the composition and structure of the zirconosilicates. *Sov. Phys. Crystallogr.* **19**, 152-156.

YAMNOVA, N.A. & EGOROV-TISMENKO, YU.K. (2000): Refined crystal structure of iron-rich triclinic astrophyllite. *Kritallographia* **N4-45**, 642-647 (in Russ.).

_____, _____ & PEKOV, I.V. (1998): Crystal structure of perraultite from the Coastal Region of the Sea of Azov. *Crystallogr. Rep.* **43**, 401-410.

WEISS, Z., RIEDER, M., CHMIELOVÁ, M. & KRAJÍČEK, J. (1985): Geometry of the octahedral coordination in micas: a review of refined structures. *Am. Mineral.* **70**, 747-757.

WOODROW, P.J. (1967): The crystal structure of astrophyllite. *Acta Crystallogr.* **22**, 673-678.